NASA Technical Memorandum 101441
AIAA-89-0752

An Experimental Investigation of Multi-Element Airfoil Ice Accretion and Resulting Performance Degradation

(NASA-TM-101441) AN EXPERIMENTAL INVESTIGATION OF MULTI-ELEMENT AIRFOIL ICE ACCRETION AND RESULTING PERFORMANCE DEGRADATION (NASA) 40 p CSCL 01A
N89-15084
Unclas
G3/02 0185093

Mark G. Potapczuk
National Aeronautics and Space Administration
Lewis Research Center
Cleveland, Ohio

and

Brian M. Berkowitz
Sverdrup Technology, Inc.
NASA Lewis Research Center Group
Cleveland, Ohio

Prepared for the
27th Aerospace Sciences Meeting
sponsored by the American Institute of Aeronautics and Astronautics
Reno, Nevada, January 9-12, 1989

NASA

AN EXPERIMENTAL INVESTIGATION OF MULTI-ELEMENT AIRFOIL ICE ACCRETION AND RESULTING PERFORMANCE DEGRADATION

Mark G. Potapczuk
National Aeronautics and Space Administration
Lewis Research Center
Cleveland, Ohio 44135

and

Brian M. Berkowitz
Sverdrup Technology, Inc.
NASA Lewis Research Center Group
Cleveland, Ohio 44135

SUMMARY

An investigation of the ice accretion patterns and performance characteristics of a multi-element airfoil was undertaken in the NASA Lewis 6- by 9-Foot Icing Research Tunnel. Several configurations of main airfoil, slat, and flaps were employed to examine the effects of ice accretion and provide further experimental information for code validation purposes. The test matrix consisted of glaze, rime, and mixed icing conditions. Airflow and icing cloud conditions were set to correspond to those typical of the operating environment anticipated for a commercial transport vehicle. Results obtained included ice profile tracings, photographs of the ice accretions, and force balance measurements obtained both during the accretion process and in a post-accretion evaluation over a range of angles of attack.

The tracings and photographs indicated substantial accretions on the slat leading edge, in gaps between slat or flaps and the main wing, on the flap leading edge surfaces, and on flap lower surfaces. Force measurements indicate the possibility of severe performance degradation, especially near C_{Lmax}, for both light and heavy ice accretions. Frost was also seen on the lower surface of the airfoil. This frost is considered to be a phenomena inherent to the IRT and is not seen in natural icing. The contribution of frost to the force components was evaluated and found to be significant.

The cruise wing configuration provided a test case for evaluation of the ice accretion and performance analysis codes presently in use. The LEWICE code was used to evaluate the ice accretion shape developed during one of the rime ice tests. The actual ice shape was then evaluated, using a Navier-Stokes code, for changes in performance characteristics. These predicted results were compared to the measured results and indicate very good agreement.

INTRODUCTION

Several studies have been completed of ice accretions and resulting performance losses for typical airfoil profiles (refs. 1 to 5). To date, most studies have been for single element airfoils such as the NACA0012 profile. The use of slats and flaps has the potential for development of significant ice

accretions at many locations on an airfoil other than the leading edge. In an effort to document these accretions and their effects on airfoil performance, a series of icing tests were performed on a multi-element model representing a Boeing 737 wing section. The configurations tested are shown in figures 1(a) to (d). Figure 1(a) represents the airfoil with slats and flaps fully retracted and corresponds to a cruise condition. Figures 1(b) to (d) have varying slat and flap conditions, as indicated, and correspond to various stages of approach. These four configurations were tested in the NASA Lewis 6- by 9-Foot Icing Research Tunnel while mounted in a horizontal position between two splitter walls, as shown in figure 2. Design and construction of the model and splitter walls was performed by Boeing Commercial Aircraft Co. in conjunction with their own fluid de-icing test conducted just prior to the test described herein.

This test was run to provide information on performance changes due to icing for a multi-element airfoil. The database produced during this test may be used to evaluate the effects of icing on slats and flaps and how their effectiveness is altered during an icing encounter. The conditions of the test were set to attempt reproduction of natural icing conditions anticipated for this airfoil during hold and approach situations, as specified in the FAR-25 specifications for commercial aircraft. This was not always possible given the restrictions imposed due to scaling and the capabilities of the IRT. In several cases, the spray durations were extended in order to accumulate ice of sufficient quantities to allow tracings to be feasible. Additionally, it was desired to obtain results for glaze, rime, and mixed conditions in order to develop an understanding of how these may impact the several configurations examined.

This test also provides substantial verification information for both LEWICE and an appropriate aerodynamic performance code, especially for future versions of these codes which may be modified for multi-element airfoils. In support of this objective ice shape tracings were taken for each test run at several locations along the airfoil span. These tracings may then be compared to LEWICE results, with the spanwise variations giving an estimate of the acceptable error bounds for the calculation. The variation of the force measurements due to the ice shape may also be used to evaluate the accuracy of the aerodynamic performance codes contemplated for use in predicting iced airfoil behavior. The performance changes were recorded both during and after the icing encounter. This will provide information for any future combined ice accretion/aero-performance code. The changes in performance as a function of time should give an indication if the ice accretion process is being modeled appropriately. This cannot be done with ice tracing methods since stopping and restarting the spray cloud would result in an ice shape somewhat different than that produced by a continuous spray for the same time period.

This test thus provided a unique opportunity to obtain important information on multi-element airfoil behavior in icing and to create a detailed database for development of advanced icing analysis methods.

TEST DESCRIPTION

This test program was conducted in the NASA Lewis 6- by 9-Foot Icing Research Tunnel (IRT). The IRT is a closed loop subsonic wind tunnel with a

solid wall test section. The maximum test section velocity is 300 mph with no blockage. The test section velocity level is normally measured using an anti-iced pitot-static probe located at the entrance to the test section. The splitter wall configuration used in this test precluded use of this probe and the velocity measurement method used will be described later. The IRT airstream temperature is controlled by a 2100 ton Freon cooling system which allows the total temperature to range between -20 and 80 °F. Atmospheric icing clouds are simulated in the tunnel by spraying water droplets into the cold airstream slightly upstream of the contraction section. Calibrated clouds may be generated with liquid-water contents ranging from 0.5 to over 2.0 g/m^3 and with volume median droplet diameters ranging from 10 to 20 μm.

The test article was a 0.18 scale model of a Boeing 737-200 ADV wing section. The model could be configured with various combinations of slat and flap extensions, as shown in figure 1. The cruise configuration had a chord length of 18 in. and a span of 60 in. The model was mounted horizontally between two splitter walls which spanned the height of the tunnel test section. The model could be rotated about its spanwise axis using a turntable mounted in the splitter walls. This allowed variation of the angle of attack both during and after the duration of the spray. For most of the test runs the model was set at 5° angle of attack (AOA) during the icing encounter. The exceptions are noted in the tables of test conditions. A diagram of the model mounted in the splitter walls is seen in figure 2.

The tunnel velocity at the location of the model was obtained by use of a calibration curve produced by Boeing during the prior ground de-icing tests. This was done by relating a static pressure probe reading located at the model location, without the model present, to that of a static pressure probe located in the ceiling upstream of the splitter walls. The output of this probe was referenced to a heated total pressure probe, also located in the tunnel ceiling, to yield the corrected free stream velocity at the model location.

Aerodynamic loads on the models were measured during and after each test run using a Boeing-designed three component force balance. One balance was mounted in each splitter wall and attached to the ends of the model. These balances allowed the measurement of the normal and axial forces and of the bending moment produced on the airfoil during the ice accretion process and during a pitch-up following the test. From these measurements, the lift, drag, and pitching moment could be determined.

This model and force balance was used in a Boeing-run De-/Anti-Icing test prior to this ice accretion test. During the De-/Anti-Icing test a problem developed in the axial force component of the left hand balance. This meant that any spanwise variation of the axial loading would lead to errors in the measurements. A simple examination of the relative magnitudes of the axial loads to either the lift or drag values indicated that an axial load imbalance could contribute to a 3 percent error in lift and as much as a 75 percent error in drag. It was decided to use the balance under these conditions and to take note of any test runs which had a nonuniform distribution of ice in the spanwise direction. It was felt that lift values would be acceptable and that if the ice accretion was uniform across the span then the drag measurements would also be meaningful.

The test conditions were selected to model cruise and approach conditions for the Boeing 737-200ADV. This consisted of determining combinations of temperature, liquid water content, and drop size within the FAR-25 envelope and scaling these conditions to the size of the model. Velocities and accretion times were also adjusted in an attempt to achieve proper scaling of the total mass of ice accreted. The attempt to remain close to actual flight conditions was done to produce realistic ice shapes and was not intended to achieve complete simulation of actual flight conditions. The main objective of these activities being to produce a database for code validation, it was decided in several runs to deviate from the simulation conditions in order to produce an ice accretion more suitable for modeling. Typically the deviations consisted of running for longer periods of time in order to accumulate enough ice to yield a suitable shape for testing the computer codes. The actual test conditions are listed in tables I to IV.

A typical test run consisted of the following steps. Prior to any ice accretion run the force coefficients versus angle of attack were determined for the clean airfoil. The spray conditions were set according to the information shown in tables I to IV. The tunnel was brought to the correct temperature and airspeed. As the spray was allowed to impinge on the airfoil, the force balance measurements were taken in order to determine changes during the encounter. These measurements were taken with the airfoil at a set angle of attack. Upon completion of the icing encounter, the force coefficients versus angle of attack were again taken to determine changes due to ice accretion and frost. After these measurements were completed, the tunnel was brought to idle and frost was removed. The tunnel was then brought back to speed and the force coefficient measurements were repeated with only the ice accretions. Finally, after this the tracings were taken at several spanwise locations on the airfoil.

After each icing test was conducted, a set of ice shape tracings were made at pre-determined locations along the span of the airfoil. A steam knife was used to cut a 0.25 in. wide slice into the ice and flush with the clean airfoil. Figure 2 shows the distance and section name for each of the five cuts. After each cut was made, a cardboard template was inserted into the cut and a tracing of the ice shape profile was made. At the beginning of these tests, it was unclear if the splitter wall configuration (fig. 2) would significantly affect the flow field downstream, especially if the splitter walls accreted a reasonable amount of ice during the run. Preliminary analysis, using both LEWICE and ARC2D, indicated that the ice accretions that would form on the leading edge of the splitter walls would be less severe than the ice accretions that would form on the leading edge of the test model. This was due to the splitter walls' greater thickness and the relative size of the ice accretion. Further investigation of the ice shape tracings along the span of the airfoil indicated that the splitter walls did not have a significant effect on the ice shapes. Thus, it appeared that the splitter walls were not disturbing the flow downstream. However, it should be noted that in three of the runs (i.e., runs 2b, 21, 22), there appeared to be a nonuniformity of the ice accretion along the span. Near section A, the ice accretions were usually less thick, but of the same general shape as the rest of the accretion. Since this occurred for both short and long duration runs, this was not considered due to the ice accretions on the splitter walls. This result seemed to be independent of temperature, velocity, or other flow conditions and thus further examination is required.

Another reason for obtaining multiple tracings of the ice accretion was to investigate the inherent variability of the icing process. As stated earlier, by obtaining ice shape tracings at various locations along the span of the airfoil and then overlaying them, a kind of "icing band" can be created. It is hoped that the LEWICE prediction will fall within this "icing band."

RESULTS AND DISCUSSION OF TEST PROGRAM

The test conditions varied from rime to mixed to glaze ice accretions. The cruise wing configuration resulted in accretions near the leading edge as is typical for single-element airfoils. The approach or flaps-extended configurations resulted in accretions at the flaps and slat leading edges and in the gaps between those surfaces and the main wing body. During many of the tests, frost was also seen to have formed on the lower surface of the airfoil. The frost was especially evident for the 15° flap configuration. Frost was seen on the upper surface only in this latter configuration. In this case, there was a gap between the slat and the main wing body. Perhaps this ice was not frost but actual ice deposition due to the flow through this gap. Frost was distinguished from the actual ice accretions by its appearance. The ice accretions had a growth pattern which indicated development in the upstream direction. The frost on the other hand seemed to have no preferred direction for growth. Instead, the frost appeared as a thin layer with a uniformly rough surface. Olsen (ref. 6) has suggested that the frost is due to a free-stream turbulence level higher than that in flight. However, since only the lower surface of the airfoil had any frost, some other reason is suspected. The effect of the frost on the airfoil performance was evaluated by taking force measurements before and after removal of the frost.

The first series of tests were performed with the cruise wing configuration. These correspond to the test conditions listed in table I. The results are presented in figures 3 to 12, which show one of the ice shape tracings for a given run, the force coefficients as a function of AOA, and the force coefficients as a function of time. In general, the ice accretion produces a premature stall and an increased drag for all of the runs. The drag values are larger over the entire range of AOA's, while the lift is not generally affected until near C_{Lmax}. This is because the ice shape does not substantially alter the pressure distribution over the airfoil until flow separation occurs, while the boundary layer is significantly altered at lower angles of attack. The moment coefficient changes from being nearly constant over the range of AOA to being a linearly increasing value with AOA until stall. Changes to this parameter reflect both the changes to the boundary layer at small AOA values and to the pressure distribution at large AOA's. All these results indicate significant changes in handling characteristics for the iced airfoil. Since the lift values do not change substantially until near C_{Lmax}, this can be an extremely important result for incorporation into flight simulators.

The first four test runs were for a duration of 5 min. The parameters varied between these runs were temperature, liquid water content (LWC), and droplet diameter. In examining the results, it is apparent that the dominant parameter is the temperature. Runs 1 and 2b were at a tunnel temperature of approximately 30 °F while runs 3 and 4b were at 13 and 10 °F, respectively.

The ice shapes developed in the former runs were glaze shapes while the latter two runs produced rime accretions. This is also reflected in the force coefficient measurements. Runs 1 and 2b had lower C_{Lmax} values, higher drag, and more distorted C_M curves than the rime ice runs. The most significant common trend for all four runs was the small ΔC_L experienced during the accretion process. The major distortion to the pressure profile near the leading edge of the airfoil has virtually no effect on the lift until the boundary layer completely detaches from the surface. The other trend to note is that the runs with the larger droplet sizes (i.e., runs 2b and 4b) had impingement limits which extended further back along the airfoil surface. This resulted in very little difference for the glaze runs and in a somewhat higher ΔC_D for run 4b as compared to run 3. The increased drag for the rime case was due to a longer stretch of rough surface in run 4b over run 3. This did not occur for the glaze cases because the flow was separated aft of the ice shape and hence the flow over the remainder of the airfoil surface was substantially the same for both these runs.

The next two runs, 5 and 6, differed only in the duration and the tunnel velocity. This amounted to a substantially larger ice accretion for run 6, as shown in figures 7 and 8. Remarkably, the change to the lift curve was actually worse for the smaller ice accretion. Perhaps the ice shape developed during run 6 acted as a leading edge slat and the increase in camber somewhat offset the loss of lift due to flow separation. Similarly, the larger ice shape of run 6 increased the drag of the airfoil much as a leading edge slat would.

Runs 7 to 10 varied in all five environmental parameters, yet some interesting trends can be noticed by selective comparison of these four runs. Runs 7 and 8 differed essentially in duration. This is seen by the larger ice accretion for run 8. Since both runs were at 15 °F, and hence in the mixed glaze and rime regime, the only difference in performance change was the increased drag for the longer duration run. The differences in lift and pitching moment were very small when compared to the difference between either run and the clean airfoil. The major difference between runs 7 and 9 was the temperature, which resulted in a mixed ice condition for the former and a rime ice condition for the latter. The rime ice shape of run 9 actually enhanced the lift characteristics for the airfoil as long as the flow remained attached. This effect was also seen in the comparison between runs 8 and 10. The rime accretion had a less deleterious effect on the lift than the mixed ice of run 8.

All 10 runs indicated a nonlinear increase in drag with respect to time. The drag appeared to vary with time to the 1/3 or 1/4 power. The lift values did not change very much at all with time due to the low angle of attack at which the ice was accreted. The moment coefficient did not seem to follow any pattern in how it changed during the accretion time. Thus, it appears that as the ice accretes it initially disturbs the boundary layer causing an increase in drag. This is most likely due to premature tripping from laminar to turbulent flow. Then, as the ice continues to grow, separation regions develop behind the ice shape and changes to the boundary layer aft of the ice shape are reduced. Further changes to lift and pitching moment are determined not by the spray duration but by the type of ice accreted with the more significant changes occurring at the warmer temperatures. This latter effect is due to changes in the overall flow pattern as opposed to alterations in the boundary

layer. These trends have been seen in other single element airfoil studies and have been reproduced in analytical simulations (refs. 14 and 15).

All 10 runs had frost on the lower surface of the airfoil. The extent of this frost varied from the first 30 percent of the airfoil to the entire lower surface. The major effect of frost is to increase the pitching moment over the entire range of AOA's. The changes in lift and drag due to frost are not as dramatic, as will be seen in the next series of runs. This indicates that the results for lift and drag previously discussed should apply whether or not the frost is present.

Runs 11 to 14 used the 5° flap configuration as shown in figure 1(c). The distinguishing characteristic of this configuration is the sharp drop in the lift at approximately 15° AOA. The icing runs covered mixed to rime ice conditions and these accretions altered the lift curve significantly. The first two runs were at 25 °F and figures 13 and 14 indicate that the sharp drop in lift is maintained for these runs with the exception that the stall occurs at a lower AOA. The two subsequent runs were at 17 and -7 °F. Figures 15 and 16 indicate that the lift curve gradually changes from the sudden loss of lift characteristic of the clean airfoil to a more gradual roll over of the lift at a somewhat lower C_{Lmax} value. The original lift curve of the airfoil is characteristic of a leading edge stall while the rime iced configuration of run 14 is characteristic of a trailing edge stall. This suggests that the mixed ice shape of runs 11 and 12 retained a small separation bubble which eventually burst at higher AOA's. The rime shapes, on the other hand, may have tripped the boundary layer and prevented the formation of the leading edge separation bubble. This idea is also supported by the drag measurements which indicate an increase in drag over all AOA values, for run 14, which is not seen in the prior three runs. Thus, as the AOA increased, the trailing edge separation became the mechanism for stall. This scenario could be examined more thoroughly through use of an aerodynamic code and that is one reason why development of a multi-element code for use in icing is important.

The other interesting feature of this set of runs is the effect of the frost. As seen in figures 13 to 16, the lift and drag values hardly altered at all due to the presence of the frost. On the other hand, the frost has a significant effect on the moment coefficient. The presence of frost tends to indicate a larger change in this value than would be suggested by the accompanying changes in lift and drag. Apparently the distribution of these forces over the surface of the airfoil is changed by the frost. Since frost is considered to be a phenomena found only in the tunnel and not in flight, tunnel tests should be evaluated with great care when extrapolating to airfoil performance in icing. This effect must also be considered when using tunnel data for code validation.

The 1° flap configuration, shown in figure 1(b), was evaluated during runs 15 to 19 and the results are shown in figures 17 to 21. The ice shapes from these runs all tended to be on the upper surface of the leading edge slat. This is quite different than the prior runs where the ice deposited at the leading edge and on the lower surface. These runs all produced lift curves with very flat tops such that stall would occur early but may not be as severe as other configurations. The exception is run number 16 which shows an earlier departure from the lift curve but no indication of the AOA at which C_{Lmax}

occurs. The drag and moment coefficient curves also appear to be affected similarly for all runs. All five of these runs were in the mixed ice regime and hence this could account for the similarities between runs.

Run 19 is particularly interesting due to the effect of frost on the lift and drag. In the range of 10° to 15° AOA the presence of frost makes a significant difference on both measurements. This run was the only one to have frost on the upper surface. The frost extended from the leading edge to the trailing edge of the main wing body. This appears to have thickened the boundary layer on the upper surface and possibly altered the pressure profile on the upper surface. This in turn resulted in the decreased lift and increased drag indicated in figure 21.

The last five runs were with the 15° flap configuration, as shown in figure 1(e). The first of these, run 20, had a data system error and hence will not be discussed. Runs 21 and 22 had the same icing conditions with only the AOA at which impingement occurred being different. There was no frost developed during either of these runs, however, there was a thin layer of accreted ice on the lower surfaces. This layer was thicker for run 22, most likely because of the increased AOA during the accretion process. The resulting changes to the force coefficients were the same for both cases until the onset of stall. The differing deposition patterns from the two runs resulted in a somewhat more severe stall condition for run 22. Runs 23 and 24 were rime ice accretions and did not exhibit the ice deposition patterns on the lower surfaces as in the prior two runs. There was, however, frost on the lower surfaces, as in previous runs with other model configurations. The signal from the force balance for these last two runs was not reading properly and was found later to be operating intermittently. Therefore, the results shown in figures 24 and 25 are considered questionable.

The variability of the ice shapes accreted during each run was examined by taking ice shape tracings at several spanwise locations as mentioned previously. The tracing locations are shown in figure 2. An example of the variability which can occur is indicated in figure 26, which shows the tracings at all six locations for run 4b. Figure 26(b) gives an indication of the limits of variability within which an ice accretion code should predict an ice shape for a given icing condition. Both the mass of ice and the extent of the ice along the surface can vary quite a bit. Examination of photographs reveal that the ice accretion pattern consisted of many ribs of ice, each extending in a chordwise direction, along the span of the model. The limits of the ice accretion, shown in figure 26(b), indicate tracings taken on and between these ribs. This run had one of the largest degrees of variability, other runs had tracings which literally overlapped. One other point to consider when evaluating these tracings is that the method of tracing a shape onto a template can itself cause some variability in determination of a given ice shape.

ICE SHAPE TRACING COMPARED TO LEWICE PREDICTION

The NASA Lewis Research Center has directed the development of an analytical ice accretion prediction code to accurately predict the growth of ice on airfoils and other geometries. Initial development of the LEWICE code was provided through a grant to the University of Dayton Research Institute. This work was an extension of earlier work by Lozowski et al. (ref. 7) and Ackley

and Templeton (ref. 8). In 1984, the LEWICE code was brought in-house for further modifications and development. This effort was conducted and concluded in 1986 by Gary Ruff (ref. 9). The LEWICE code consists of three main modules: (1) a Hess-Smith two-dimensional potential flow panel method to calculate the flow field about an arbitrary two dimensional body, (2) a particle trajectory code developed by FWG that calculates the water droplet paths and their resulting impingement pattern on the body, and (3) an ice accretion module that solves the quasi-steady energy balance equation. The energy balance equation first proposed by Messinger (ref. 10) accounts for the governing heat and mass transfer process occurring during the icing process. The LEWICE code is unique in that it has a time-stepping capability to grow the ice unlike other ice accretion codes which grow the ice in one time step. With a time-stepping code the flow field and water droplet trajectories can be updated as ice is accreted on the leading edge thus disturbing the flow field. This should result in a more accurate representation of the flow field as the ice accretion is formed. Inputs required by LEWICE include the cloud properties such as liquid water content (LWC) and droplet size (MVD) and the icing conditions which include the freestream velocity (V_∞), static air temperature (T_S), static pressure (P_S), and the angle of attack (AOA). A detailed description of the code and the method of analysis can be found in the LEWICE User's Manual.

To illustrate the utility of the LEWICE model, run 4b was selected as an example case in which the LEWICE predicted ice shape will be compared to the experimental ice shape. Run 4b was selected for several reasons. First, the current LEWICE model has been tested with single element airfoils only. Therefore, comparisons were limited to the cruise wing configuration. Secondly, run 4b had a relatively large ice accretion and the performance characteristics of the airfoil indicated a significant degradation in lift between the clean and the iced airfoil geometries. Therefore, it was felt that this would be an interesting case not only for LEWICE but for ARC2D as well. Input values are given in Tables I to IV for each of the runs conducted in this test. Table I shows the values used for run 4b. Since LEWICE requires static temperature and pressure, the total temperature and pressure were adjusted to obtain static conditions. An airfoil chord of 0.457 m was used along with an equivalent sandgrain roughness (k) of 0.0008 m. This value of k was determined from reference 9, appendix F and is a function of the velocity, temperature, and liquid water content. For this comparison, two 2.5-min time-steps were used to accrete the resultant ice shape. Figure 27 shows the predicted ice shape (solid line) and the experimental ice shape (dashed line) for run 4b. Generally speaking, LEWICE does a good job of predicting the ice shape. The calculated impingement limits and the mass of ice accreted agree quite well. However, the LEWICE generated ice shape does not predict the "point" that exists on the experimental shape near the leading edge of the ice shape. The LEWICE prediction can also be compared to the icing band discussed in the previous section, which indicates the variability of the ice shape along the span of the airfoil. The LEWICE prediction stays within the band everywhere except along the lower surface of the ice shape. This is not a difficulty in predicting the impingement limits, however the bulge in the LEWICE predicted shape on the lower surface may be preventing impingement in the region just aft.

For the most part, figure 27 is typical of other LEWICE comparisons with both artificial and natural ice shape data. As other studies have indicated (ref. 11), LEWICE often provides a reasonable engineering approximation for most ice shapes. In general, LEWICE predictions agree more favorably with rime

ice accretions than with glaze ice accretions, although results for glaze ice accretions are encouraging. There appears to be no set of icing conditions in which LEWICE consistently does a poor job. However, poorer agreement will usually result for extreme cases such as large horn shaped ice at high angles of attack. Recent high speed films by Olsen (ref. 12) indicate that there may be some gross errors in the modeling of the physics of the ice accretion process, especially in the glaze ice regimes. This would explain the less than satisfactory results obtained from LEWICE for glaze ice comparisons. In addition, Hansman and Turnock (ref. 13) have proposed a multi-zone approach to the ice accretion process based on their experimental studies of the surface water behavior for glaze ice accretions. This and other work suggests that changes to the existing model should be made to try to improve the accuracy of the predictions. Investigation of these and other proposed modifications to the LEWICE model are currently being undertaken by the NASA Lewis Aircraft Icing Analysis Program.

PERFORMANCE CHANGE EVALUATION USING NAVIER-STOKES CODE

Evaluation of the changes to airfoil performance resulting from ice deposition is a major goal in development of an icing analysis capability. Presently two alternate methods are being considered. These are the interactive boundary-layer approach of Cebeci (ref. 14) and the use of a Navier-Stokes code (ref. 15). For this work, the Navier-Stokes code, ARC2D, was used to evaluate one of the test runs for changes in performance characteristics. Since the present version of the code has only been tried for single element airfoils, the cruise configuration was evaluated. Run 4b was selected, since this run was also chosen for use in the LEWICE evaluation. This will indicate the nature of future evaluations of the remaining test runs.

The results for C_L and C_D are shown in figure 28. The figures indicate the comparisons between ARC2D and experiment for both the clean airfoil and the iced airfoil. The calculations were extended to an AOA corresponding to C_{Lmax}. For the clean airfoil, the agreement is excellent up to this point while at AOA's above C_{Lmax} the solution does not converge. Evaluation of this airfoil at these higher AOA values will require further examination of such parameters as grid spacing or specification of the surface geometry. The results for the iced airfoil are not as good, with the code underpredicting the lift. Again, further grid refinement may be required to adequately model this geometry. The use of tools such as an unstructured mesh are presently being examined. These results do indicate, however, that an actual ice shape geometry can be evaluated for changes in performance characteristics.

CONCLUSIONS

This series of tests was designed to provide code verification information in support of development of multi-element capabilities for ice accretion codes and for aerodynamic performance codes. The test results provide a wide variety of conditions and should serve as a set of useful test cases. The single element cases help to ensure confidence in the codes capabilities prior to modification for multi-element geometries.

The test results indicate that the changes in performance characteristics are most affected by the temperature and duration of the ice accretion. The warmer temperatures, leading to glaze ice conditions, tend to produce the largest loss of lift. The duration of the accretion does not influence the changes to the lift once the accretion has developed beyond some minimal size. The drag increase is not so dependent on temperature while it does increase significantly with time. The drag rise was not seen to be linear but developed according to a 1/3 to 1/4 power law. This indicated a change from friction dominated drag to pressure dominated drag. The moment coefficient normally increased as a result of the accretion. This tended to produce a less stable condition for the airfoil as the tendency towards stall was enhanced.

Another significant result was documentation of the effect of frost. Frost was identified as ice that developed with no preferred growth direction as opposed to accreted ice which tended to grow upstream. Typically, the frost grew on the first 30 to 40 percent of the lower surface of the airfoil. The frost did not alter the lift or drag in many cases but did change the pitching moment. This indicates that the pressure profile was altered somewhat but more in distribution than in magnitude. It is important to insure that frost is removed prior to measurement of iced airfoil performance values in order to more accurately recreate natural icing conditions.

Variability of the ice accretion as a function of spanwise location was documented by taking ice profile tracings at several locations during each test run. Results indicated that the ice shape profiles could be quite different even when visual inspection indicated uniform ice growth. This suggests that ice accretion codes, such as LEWICE, be compared to more than one specific profile for a given set of icing conditions. As such, the LEWICE comparison to run 4b indicated that the code prediction fell within the icing band constructed from all the tracing of that test. The test also provided data useful for evaluation of performance change calculations with a multi-element airfoil code.

REFERENCES

1. Gray, V.H. and von Glahn, U.H., "Effects of Ice and Frost Formations on Drag of NACA 65-212 Airfoil for Various Modes of Thermal Ice Protection," NACA TN-2962, 1953.

2. Gray, V.H. and von Glahn, U.H., "Aerodynamic Effects Caused by Icing of an Unswept NACA 65A004 Airfoil," NACA TN-4151, 1957.

3. Bragg, M.B., Zaguli, R.J., and Gregorek, G.M., "Wind Tunnel Evaluation of Airfoil Performance Using Simulated Ice Shapes," NASA CR-167960, 1982.

4. Korkan, K.D., Cross, E.J., Jr., and Cornell, C.C., "Experimental Study of Performance Degradation of a Model Helicopter Main Rotor with Simulated Ice Shape," AIAA Paper No. 84-0184, Jan. 1984.

5. Bragg, M.B., "An Experimental Study of the Aerodynamics of a NACA 0012 Airfoil with a Simulated Glaze Ice Accretion," NASA CR-179897, 1986.

6. Olsen, W., Shaw, R., and Newton, J., "Ice Shapes and the Resulting Drag Increase for a NACA 0012 Airfoil," NASA TM-83556, 1983.

7. Lozowski, E.P., Stallabrass, J.R., and Hearty, P.F., "The Icing of an Unheated Non-Rotating Cylinder. Pt. 1: A Simulation Model," J. Clim. Appl. Meteorol., Vol. 22, No. 12, Dec. 1983, pp. 2053-2062.

8. Ackley, S.F., and Templeton, M.K., "Computer Modeling of Atmospheric Ice Accretion," CRREL Report 79-4, Mar. 1979.

9. Ruff, G.A., "LEWICE: A User's Manual," To be published as a NASA CR in 1988.

10. Messinger, B.L., "Equilibrium Temperature of an Unheated Icing Surface as a Function of Airspeed," J. Aeronaut. Sci., Vol. 20, No. 1, Jan. 1953, pp. 29-42.

11. Berkowitz, B.M. and Riley, J.T., "Analytical Ice Shape Predictions for Flight in Natural Icing Conditions," NASA CR-182234, 1989.

12. Olsen, W. and Walker, E., "Experimental Evidence for Modifying the Current Physical Model for Ice Accretion on Aircraft Surfaces," NASA TM-87184, 1986.

13. Hansman, R.J., Jr., and Turnock, S.R., "Investigation of Surface Water Behavior During Glaze Ice Accretion," AIAA Paper 88-0015, Jan. 1988.

14. Cebeci, T., "Calculation of Flow Over Iced Airfoils," AIAA Paper 88-0112, Jan. 1988.

15. Potapczuk, M.G., "Numerical Analysis of a NACA 0012 Airfoil with Leading Edge Ice Accretions," AIAA Paper 87-0101, Jan. 1987.

TABLE I. - TEST CONDITIONS FOR THE CRUISE WING CONFIGURATION

Run number	Duration, min	Temperature, °F	Velocity, ft/s	LWC, g/m^3	MVD, μm
1	5	30	158	1.49	14
2b	↓	28	↓	1.4	17
3	↓	13	↓	.9	14
4b	↓	10	↓	1.13	17
5	2	20	↓	.7	14
6	13	20	240	.7	14
7	5	16	235	1.0	12.5
8	8	15	236	.8	14
9	5	-16	154	.87	17.1
10	8	-19	152	1.38	16

TABLE II. - TEST CONDITIONS FOR THE 5° FLAP CONFIGURATION

Run number	Duration, min	Temperature, °F	Velocity, ft/s	LWC, g/m^3	MVD, μm
11	4	24	158	0.48	13.4
12	11	25	158	.46	12
13	8	17	158	.42	13.4
14	8	-7	157	.9	14

TABLE III. - TEST CONDITIONS FOR THE 1° FLAP CONFIGURATION

Run number	Duration, min	Temperature, °F	Velocity, ft/s	LWC, g/m^3	MVD, μm
15	5	28	158	0.92	14.4
[a]16	10	27	158	.92	↓
17	↓	26	159	.92	
[a]18		18	158	.9	
19		19	157	.9	

[a]These runs were accreted with the airfoil at 0° AOA.

TABLE IV. - TEST CONDITIONS FOR THE 15° FLAP CONFIGURATION

Run number	Duration, min	Temperature, °F	Velocity, ft/s	LWC, g/m^3	MVD, μm
[a,b]20	8	28	158	0.92	14.4
21	8	28	158	.92	14.4
[c]22	8	29	158	.92	14.4
[a]23	6	-3	161	.62	12.2
24	6	-9	158	.62	12.2

[a]These runs were accreted with the airfoil at 0° AOA.
[b]Force measurements lost due to data system error.
[c]This run was accreted with the airfoil at 8° AOA.

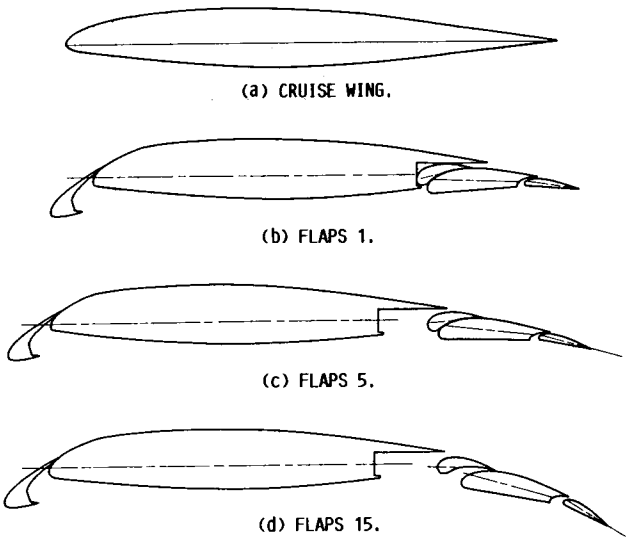

FIGURE 1. - MULTI-ELEMENT AIRFOIL CONFIGURATIONS EMPLOYED DURING ICE ACCRETION TEST PROGRAM.

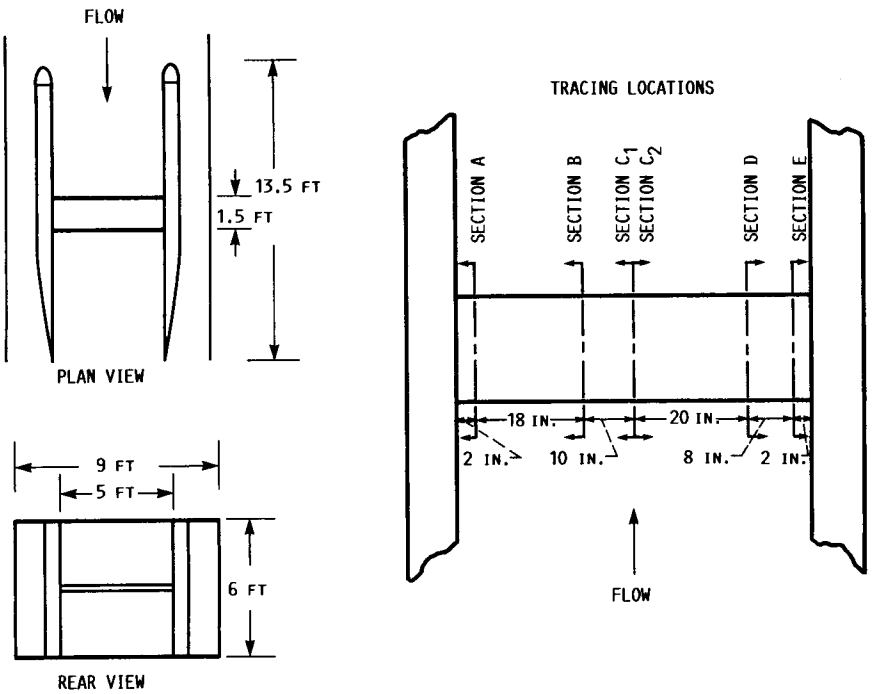

FIGURE 2. - SPLITTER WALL CONFIGURATIONS FOR 2D WING MODEL.

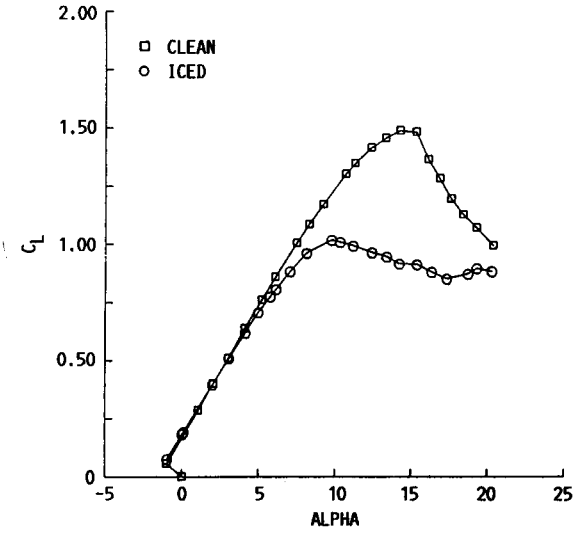

(a) C_L VERSUS AOA.

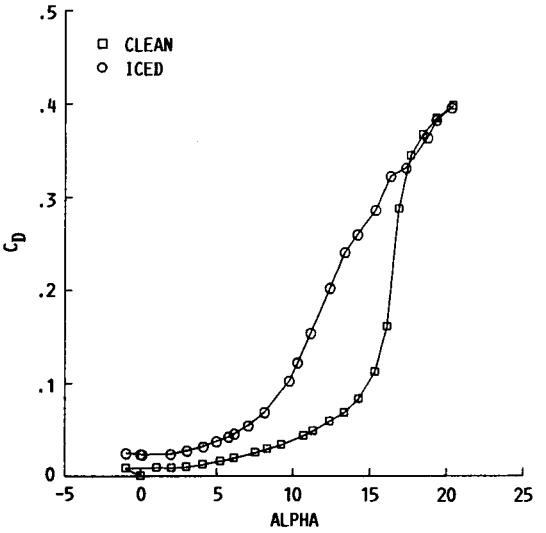

(b) C_D VERSUS AOA.

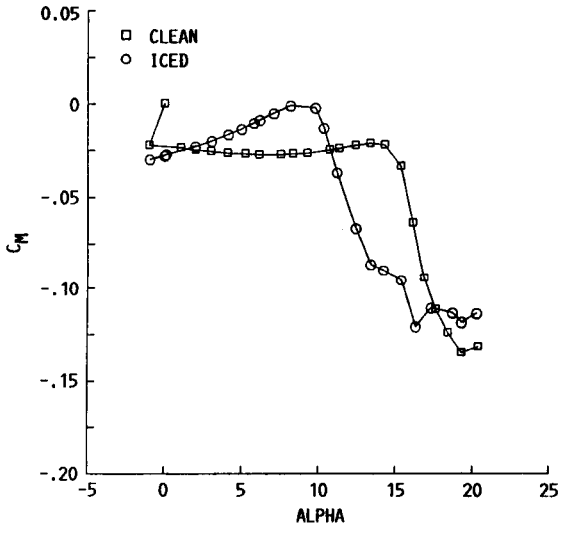

(c) C_M VERSUS AOA.

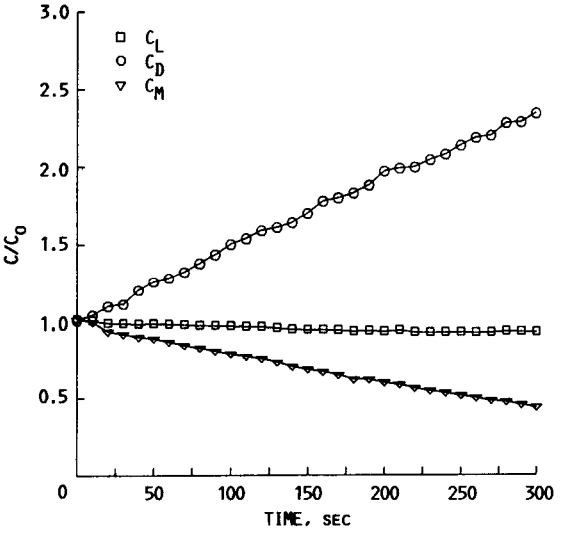

(d) RATIO OF FORCE COEFFICIENTS/FORCE COEFFICIENT OF CLEAN AIRFOIL VERSUS TIME.

FIGURE 3. - ICE SHAPE TRACINGS AND FORCE BALANCE MEASUREMENTS FOR RUN NUMBER 1.

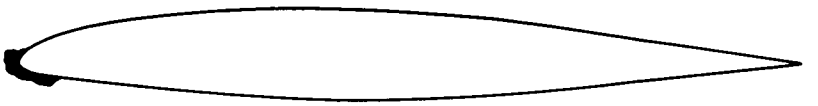

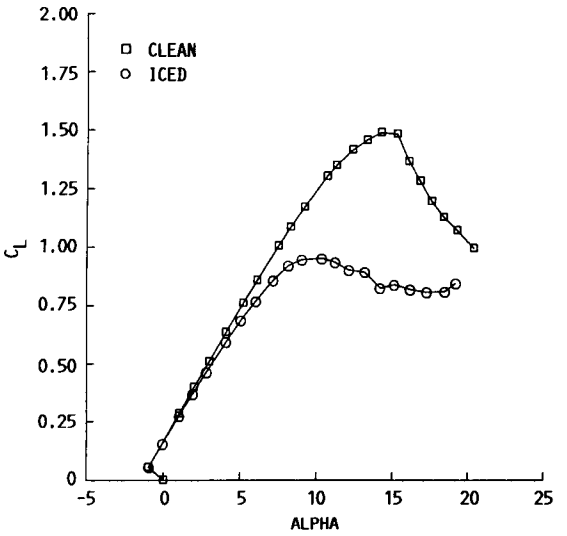

(a) C_L VERSUS AOA.

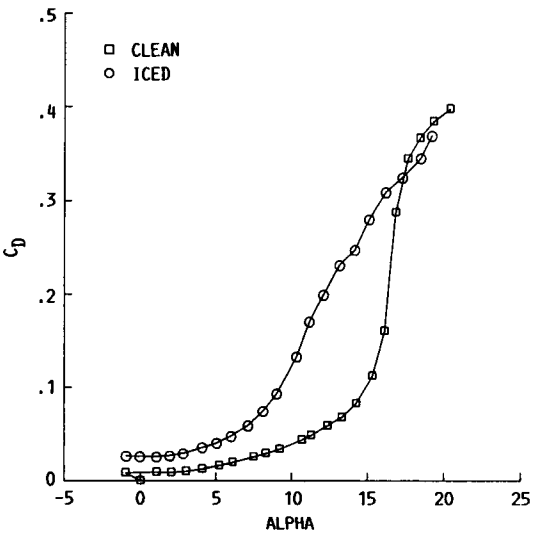

(b) C_D VERSUS AOA.

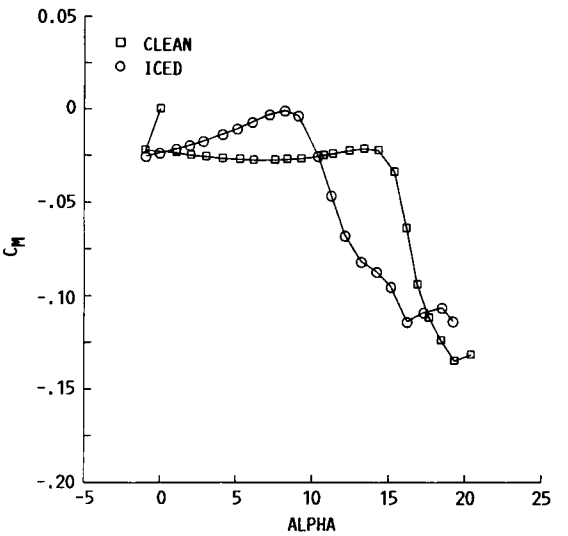

(c) C_M VERSUS AOA.

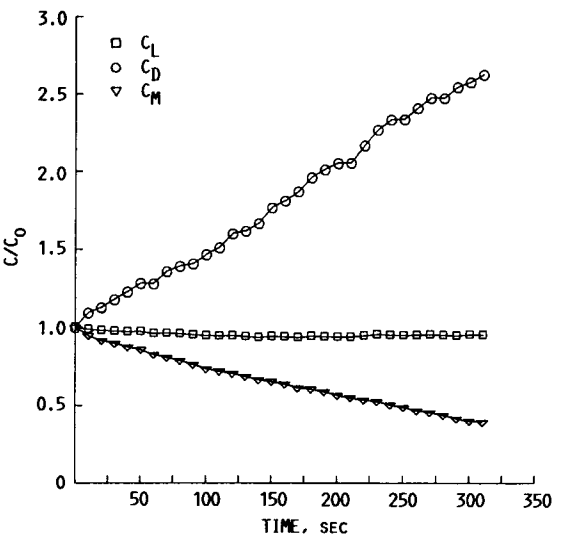

(d) RATIO OF FORCE COEFFICIENTS/FORCE COEFFICIENT OF CLEAN AIRFOIL VERSUS TIME.

FIGURE 4. - ICE SHAPE TRACINGS AND FORCE BALANCE MEASUREMENTS FOR RUN NUMBER 2 .

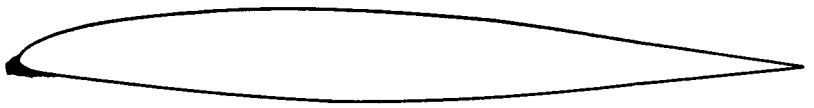

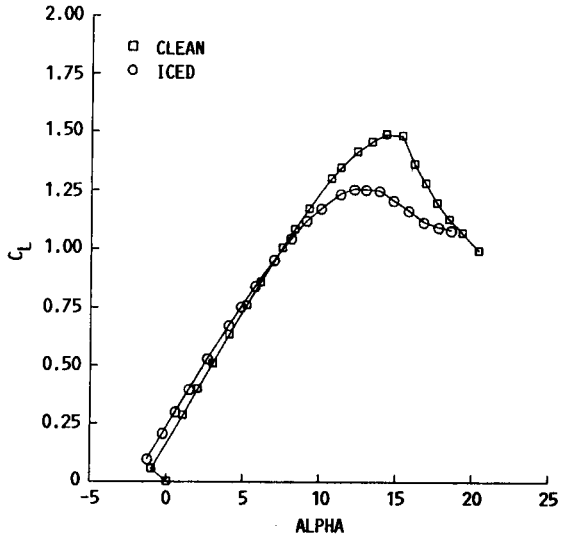

(a) C_L VERSUS AOA.

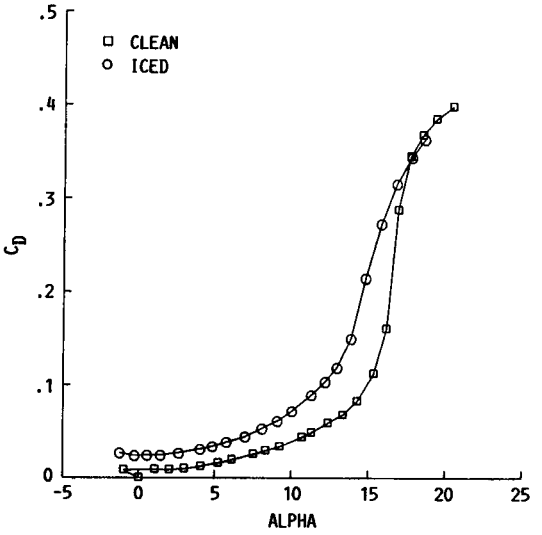

(b) C_D VERSUS AOA.

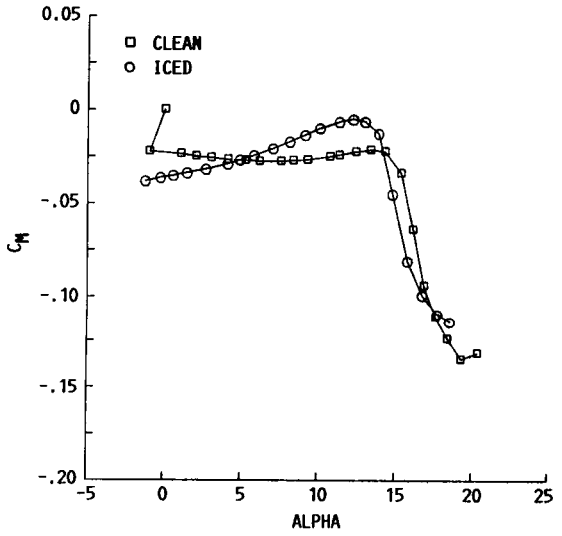

(c) C_M VERSUS AOA.

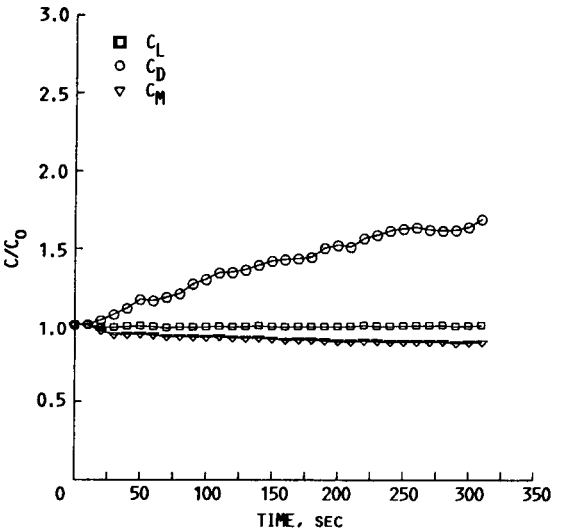

(d) RATIO OF FORCE COEFFICIENTS/FORCE COEFFICIENT OF CLEAN AIRFOIL VERSUS TIME.

FIGURE 5. - ICE SHAPE TRACINGS AND FORCE BALANCE MEASUREMENTS FOR RUN NUMBER 3.

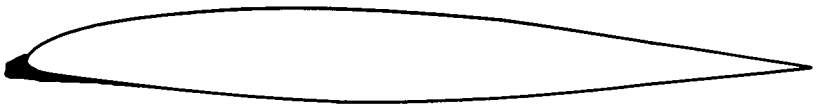

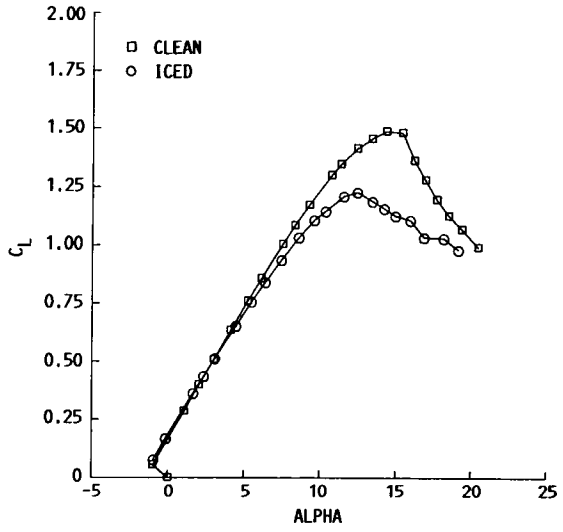

(a) C_L VERSUS AOA.

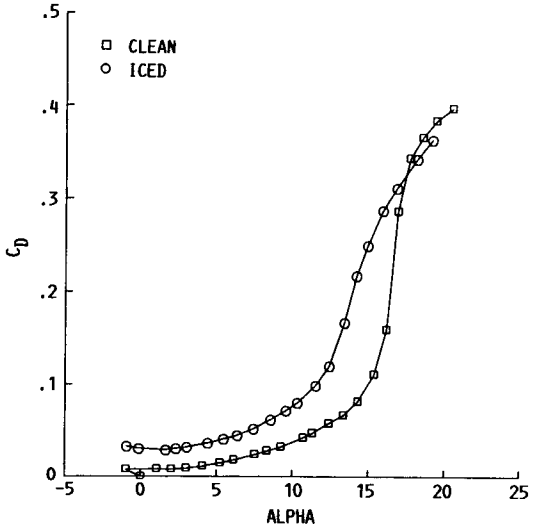

(b) C_D VERSUS AOA.

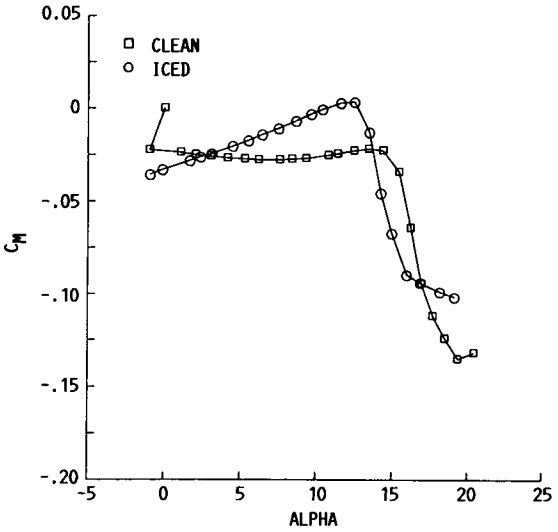

(c) C_M VERSUS AOA.

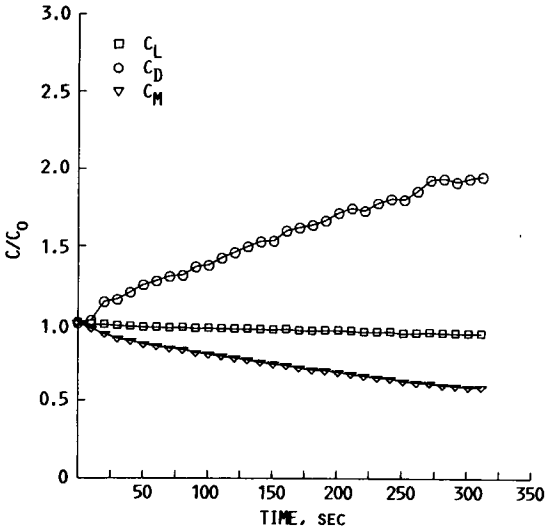

(d) RATIO OF FORCE COEFFICIENTS/FORCE COEFFICIENT OF CLEAN AIRFOIL VERSUS TIME.

FIGURE 6. - ICE SHAPE TRACINGS AND FORCE BALANCE MEASUREMENTS FOR RUN NUMBER 4b.

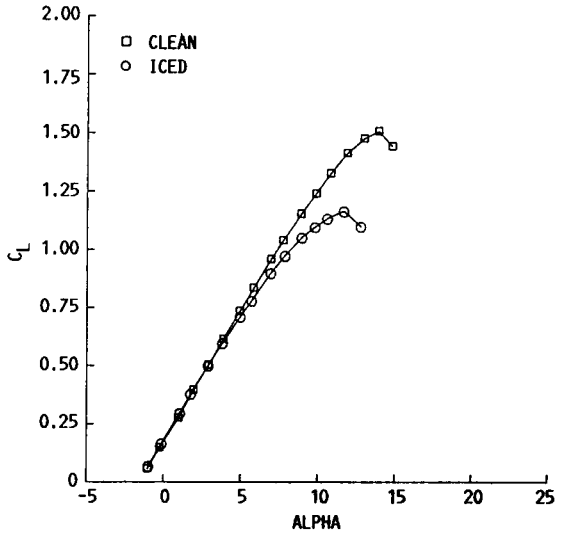

(a) C_L VERSUS AOA.

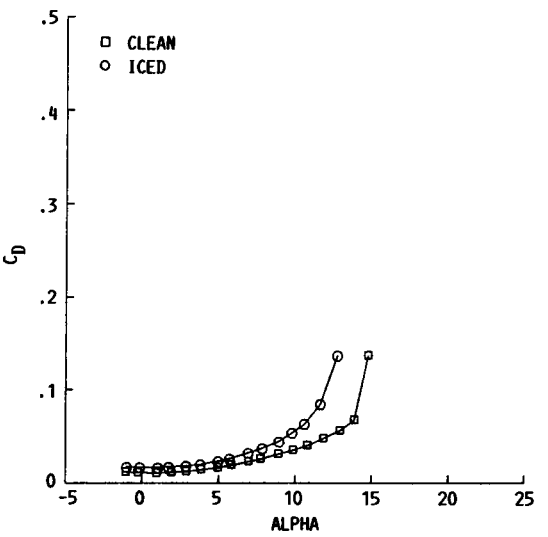

(b) C_D VERSUS AOA.

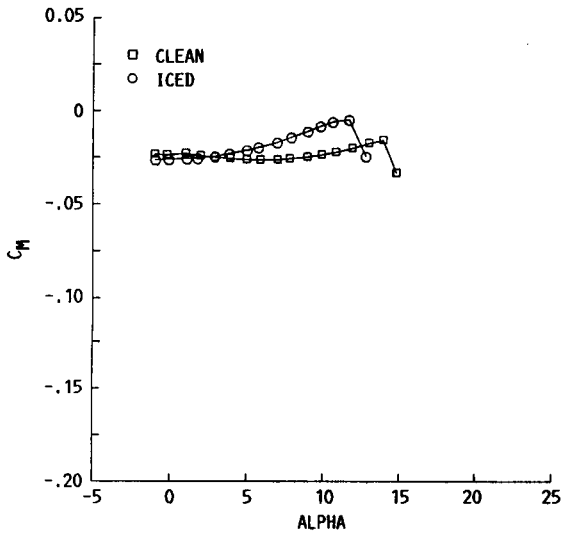

(c) C_M VERSUS AOA.

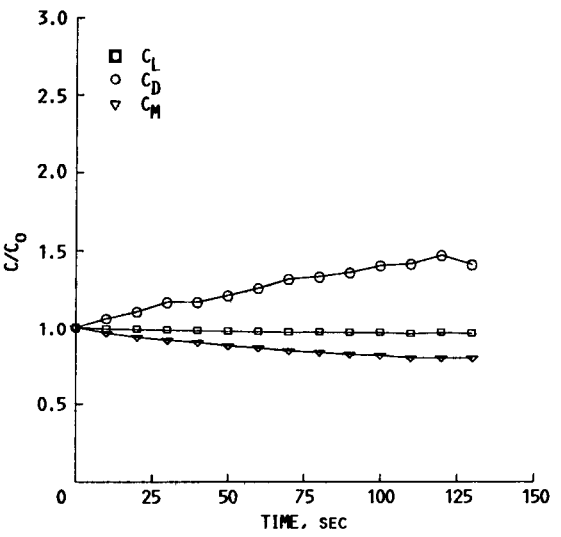

(d) RATIO OF FORCE COEFFICIENTS/FORCE COEFFICIENT OF CLEAN AIRFOIL VERSUS TIME.

FIGURE 7. - ICE SHAPE TRACINGS AND FORCE BALANCE MEASUREMENTS FOR RUN NUMBER 5.

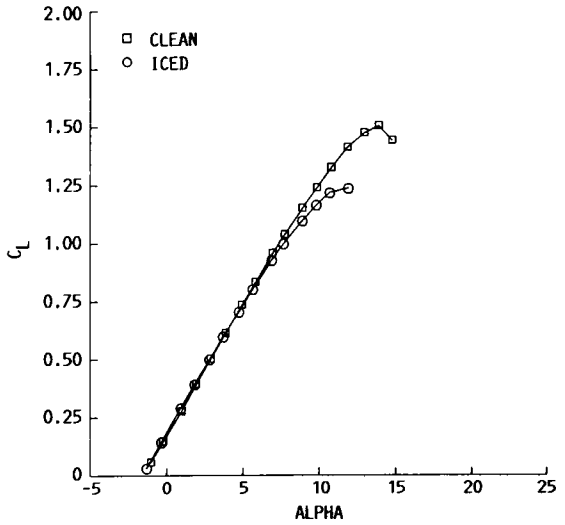

(a) C_L VERSUS AOA.

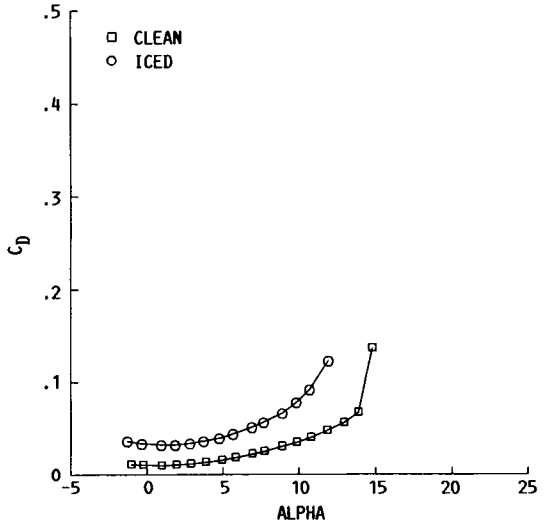

(b) C_D VERSUS AOA.

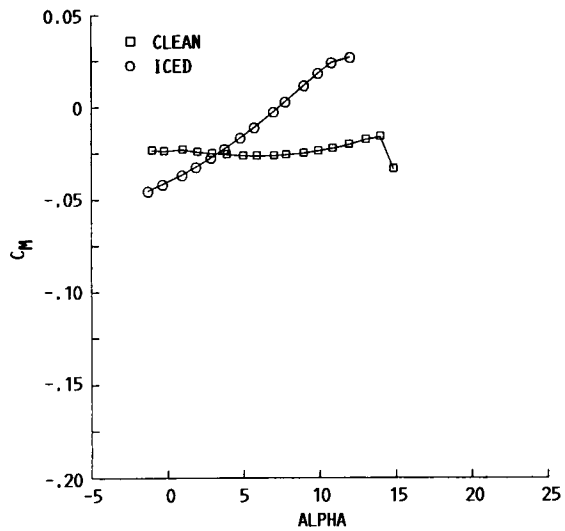

(c) C_M VERSUS AOA.

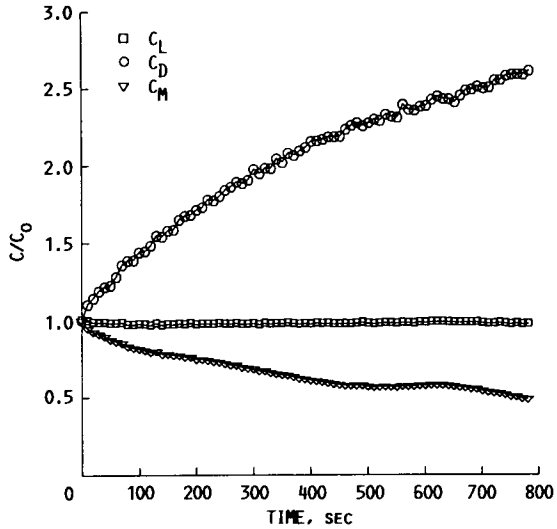

(d) RATIO OF FORCE COEFFICIENTS/FORCE COEFFICIENT OF CLEAN AIRFOIL VERSUS TIME.

FIGURE 8. - ICE SHAPE TRACINGS AND FORCE BALANCE MEASUREMENTS FOR RUN NUMBER 6.

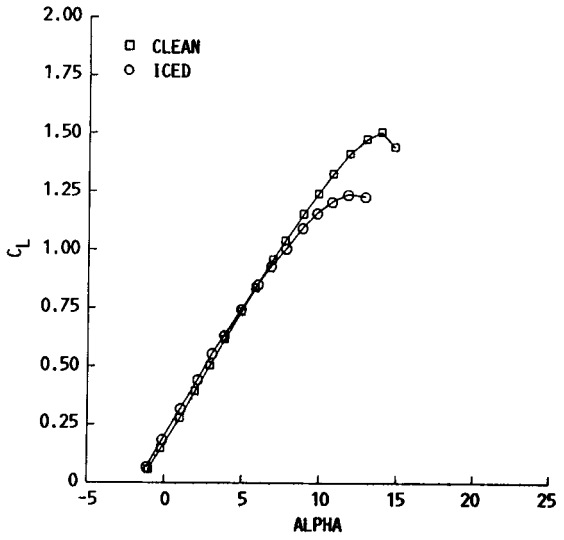

(a) C_L VERSUS AOA.

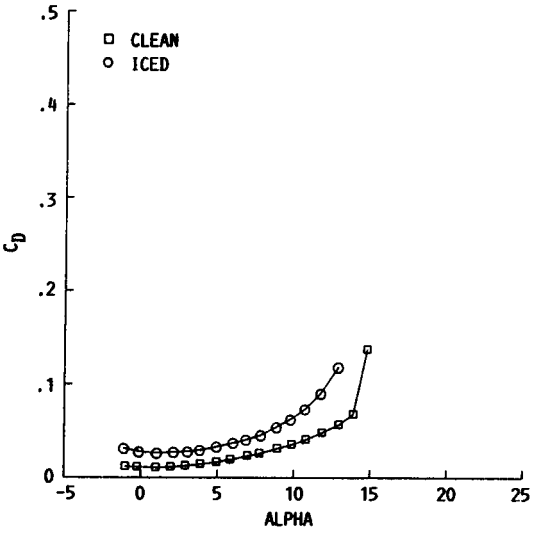

(b) C_D VERSUS AOA.

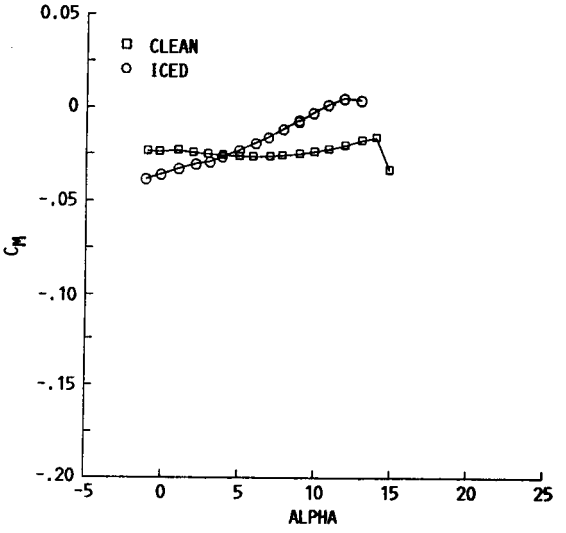

(c) C_M VERSUS AOA.

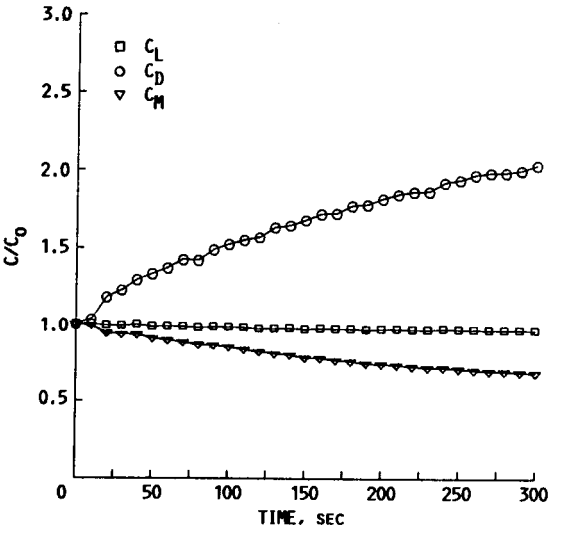

(d) RATIO OF FORCE COEFFICIENTS/FORCE COEFFICIENT OF CLEAN AIRFOIL VERSUS TIME.

FIGURE 9. - ICE SHAPE TRACINGS AND FORCE BALANCE MEASUREMENTS FOR RUN NUMBER 7.

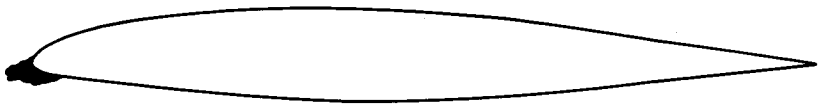

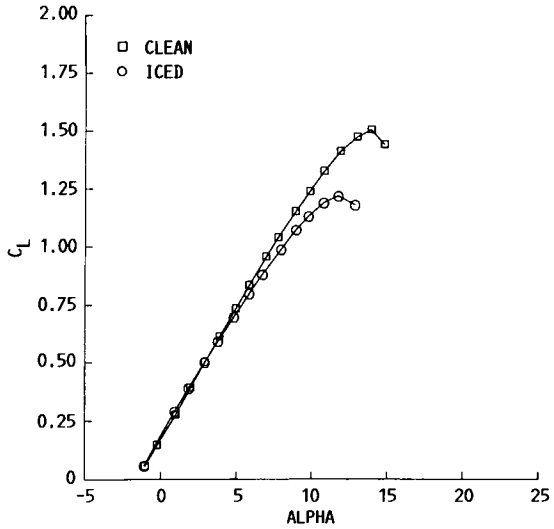

(a) C_L VERSUS AOA.

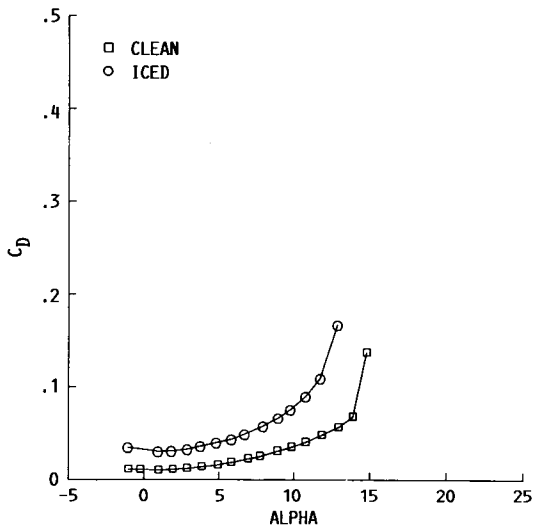

(b) C_D VERSUS AOA.

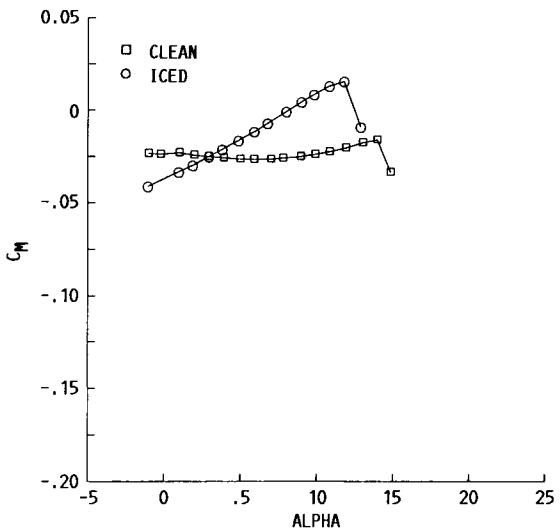

(c) C_M VERSUS AOA.

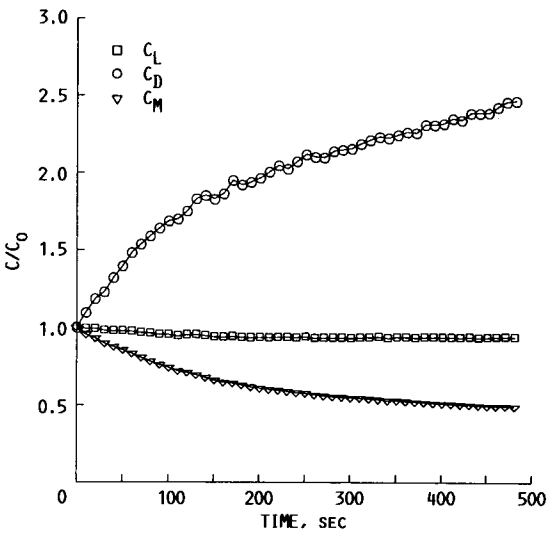

(d) RATIO OF FORCE COEFFICIENTS/FORCE COEFFICIENT OF CLEAN AIRFOIL VERSUS TIME.

FIGURE 10. - ICE SHAPE TRACINGS AND FORCE BALANCE MEASUREMENTS FOR RUN NUMBER 8.

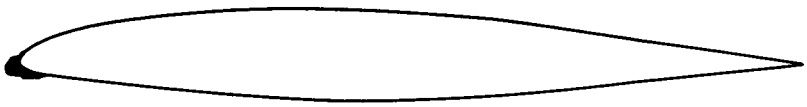

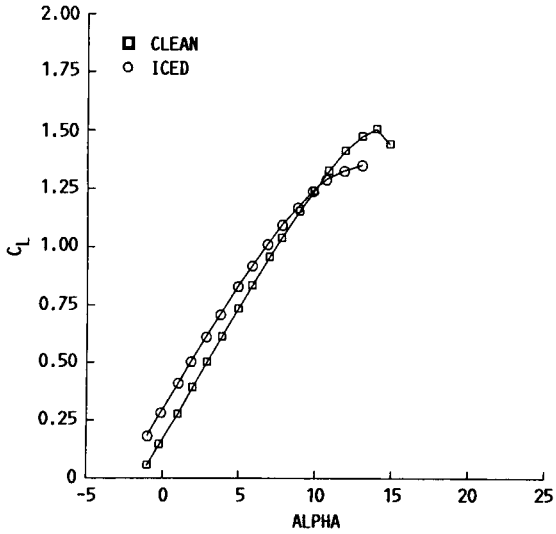

(a) C_L VERSUS AOA.

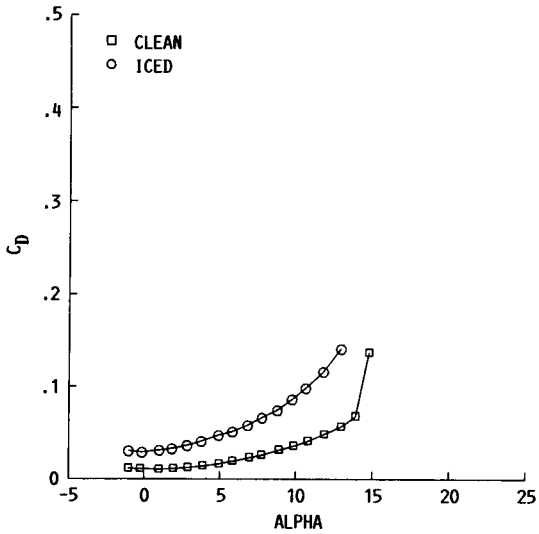

(b) C_D VERSUS AOA.

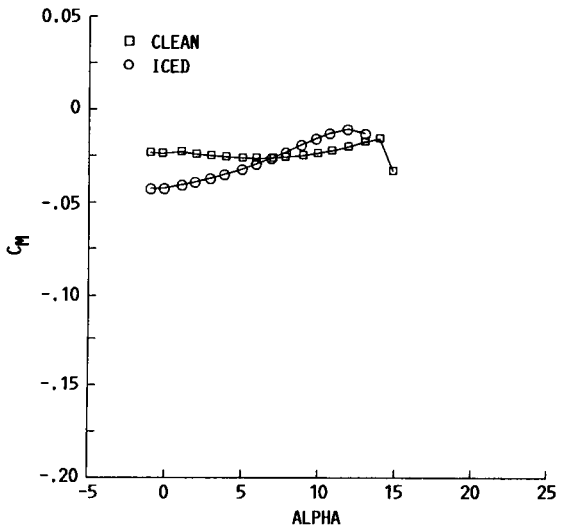

(c) C_M VERSUS AOA.

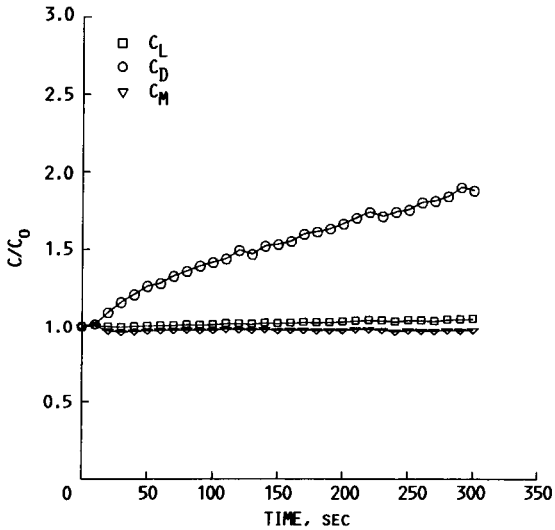

(d) RATIO OF FORCE COEFFICIENTS/FORCE COEFFICIENT OF CLEAN AIRFOIL VERSUS TIME.

FIGURE 11. - ICE SHAPE TRACINGS AND FORCE BALANCE MEASUREMENTS FOR RUN NUMBER 9.

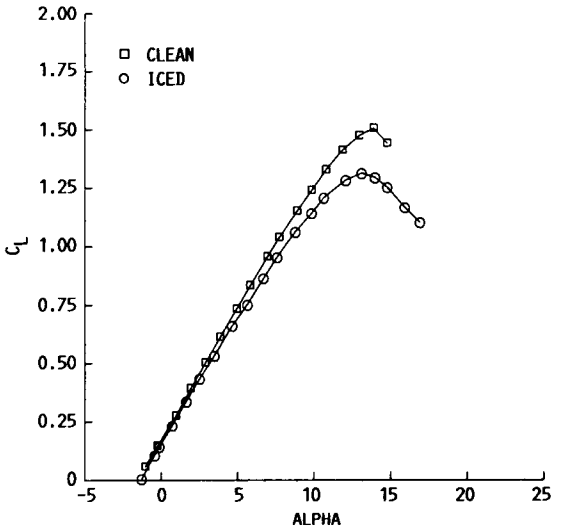

(a) C_L VERSUS AOA.

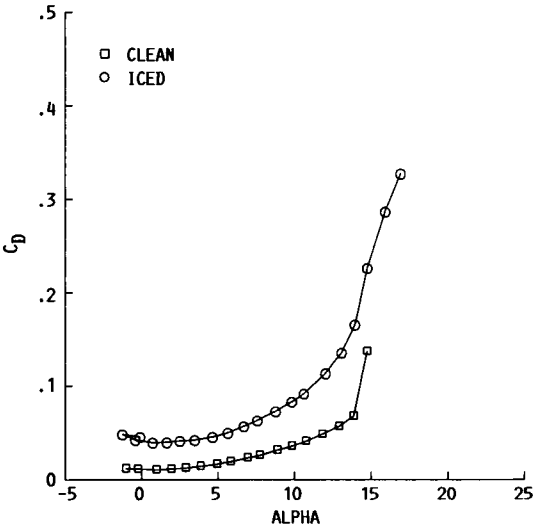

(b) C_D VERSUS AOA.

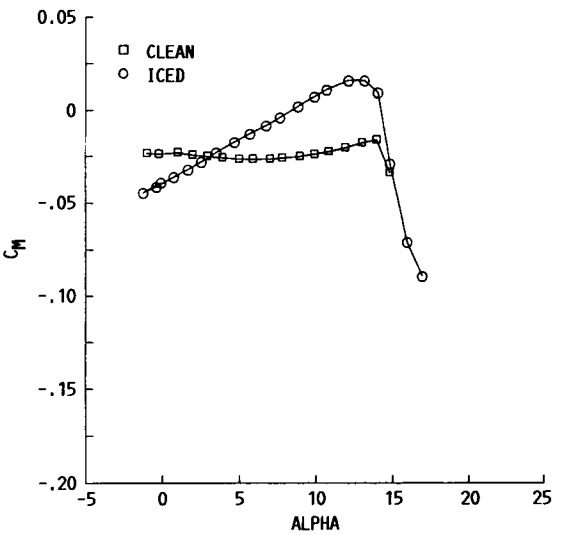

(c) C_M VERSUS AOA.

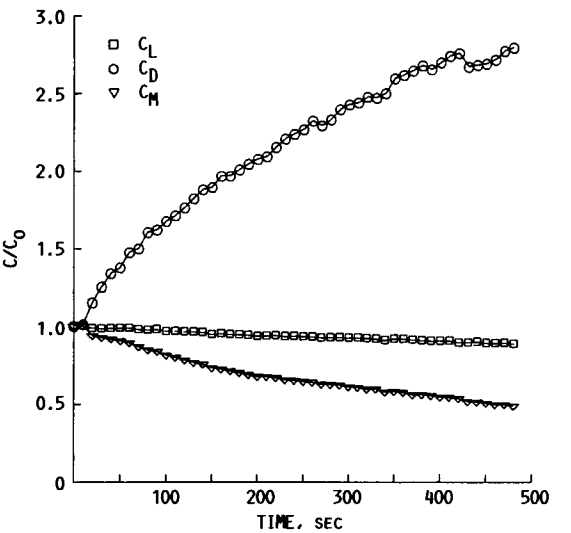

(d) RATIO OF FORCE COEFFICIENTS/FORCE COEFFICIENT OF CLEAN AIRFOIL VERSUS TIME.

FIGURE 12. - ICE SHAPE TRACINGS AND FORCE BALANCE MEASUREMENTS FOR RUN NUMBER 10.

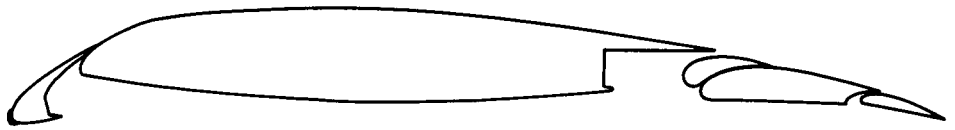

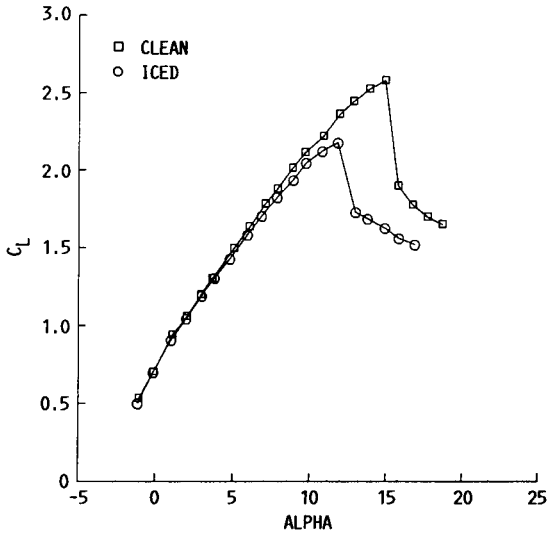

(a) C_L VERSUS AOA.

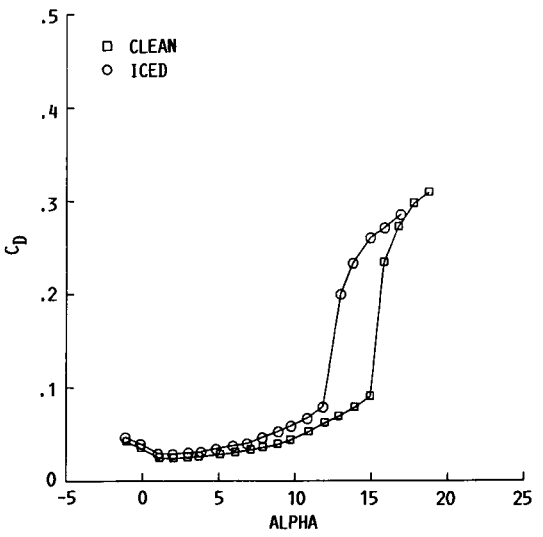

(b) C_D VERSUS AOA.

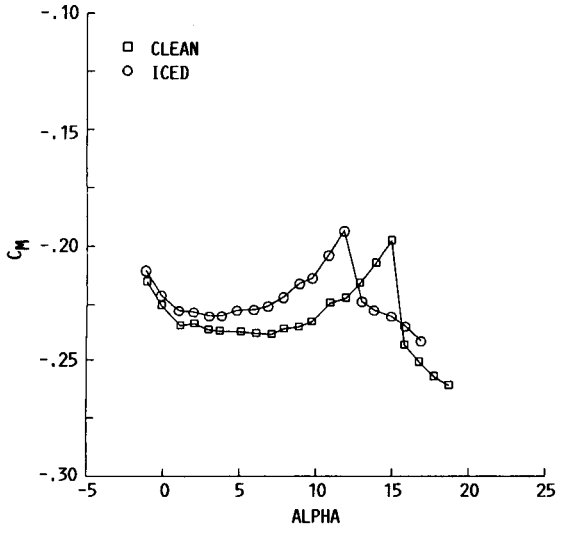

(c) C_M VERSUS AOA.

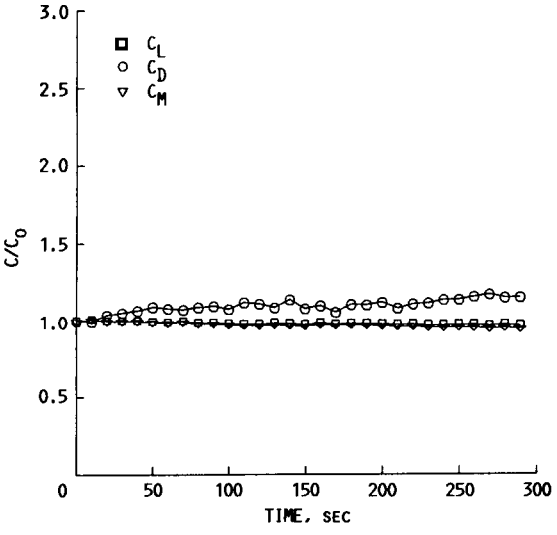

(d) RATIO OF FORCE COEFFICIENTS/FORCE COEFFICIENT OF CLEAN AIRFOIL VERSUS TIME.

FIGURE 13. - ICE SHAPE TRACINGS AND FORCE BALANCE MEASUREMENTS FOR RUN NUMBER 11.

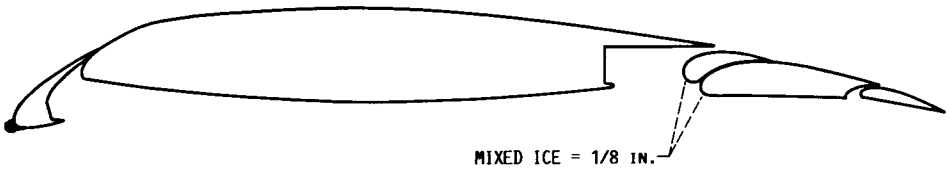

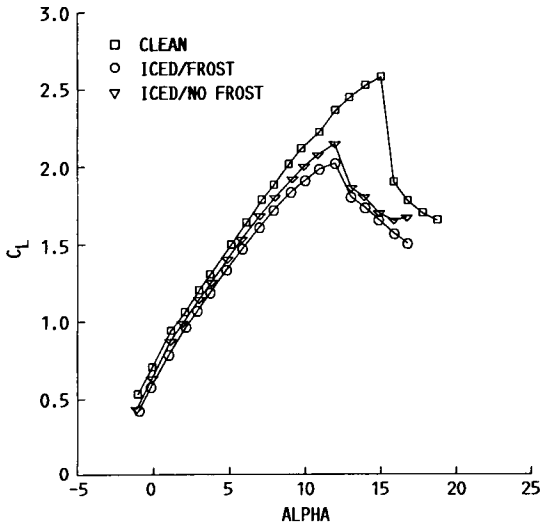

(a) C_L VERSUS AOA.

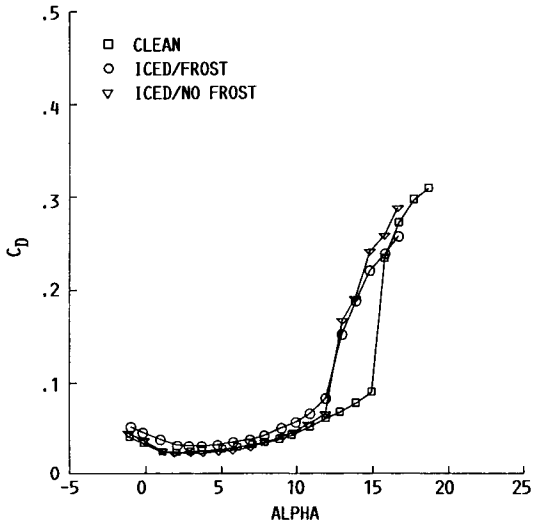

(b) C_D VERSUS AOA.

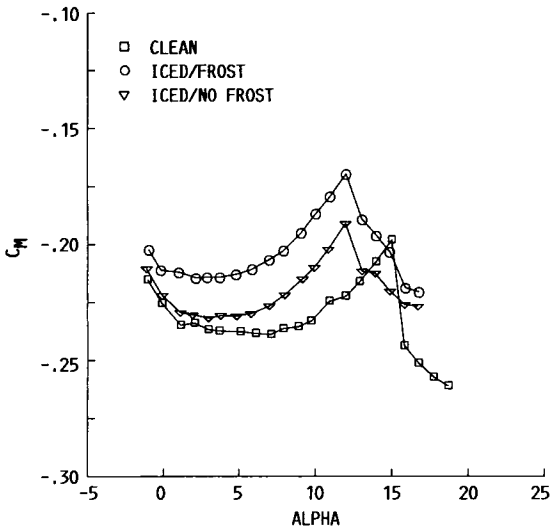

(c) C_L VERSUS AOA.

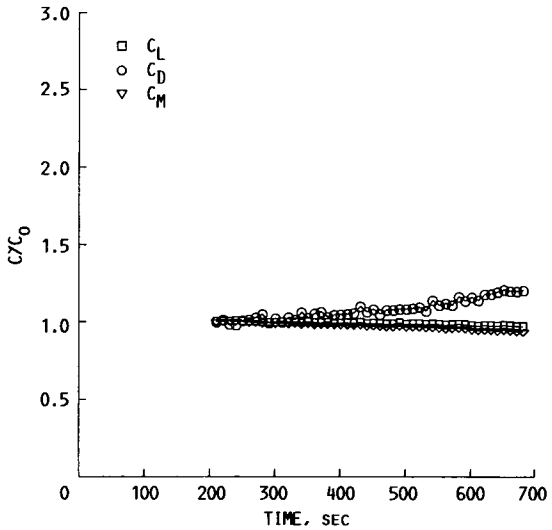

(d) RATIO OF FORCE COEFFICIENTS/FORCE COEFFICIENT OF CLEAN AIRFOIL VERSUS TIME.

FIGURE 14. - ICE SHAPE TRACINGS AND FORCE BALANCE MEASUREMENTS FOR RUN NUMBER 12.

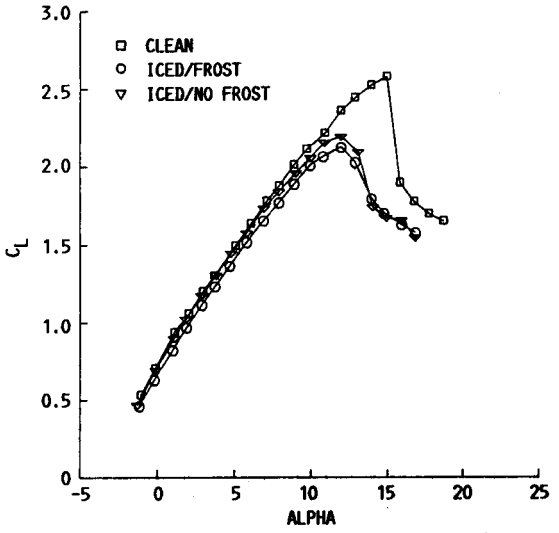

(a) C_L VERSUS AOA.

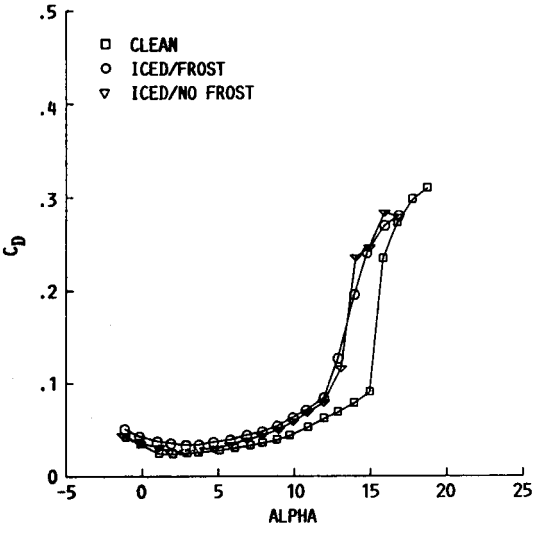

(b) C_D VERSUS AOA.

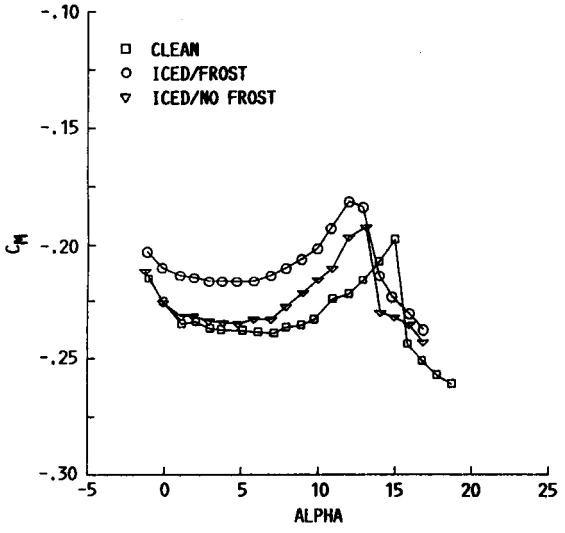

(c) C_M VERSUS AOA.

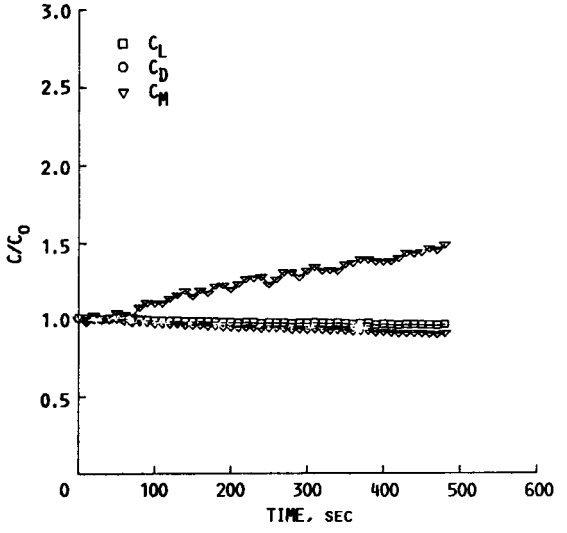

(d) RATIO OF FORCE COEFFICIENTS/FORCE COEFFICIENT OF CLEAN AIRFOIL VERSUS TIME.

FIGURE 15. - ICE SHAPE TRACINGS AND FORCE BALANCE MEASUREMENTS FOR RUN NUMBER 13.

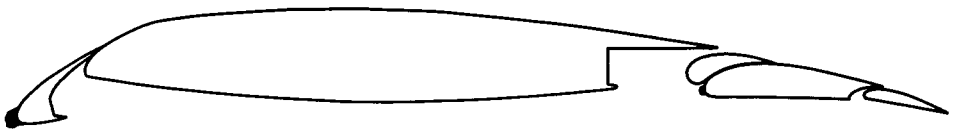

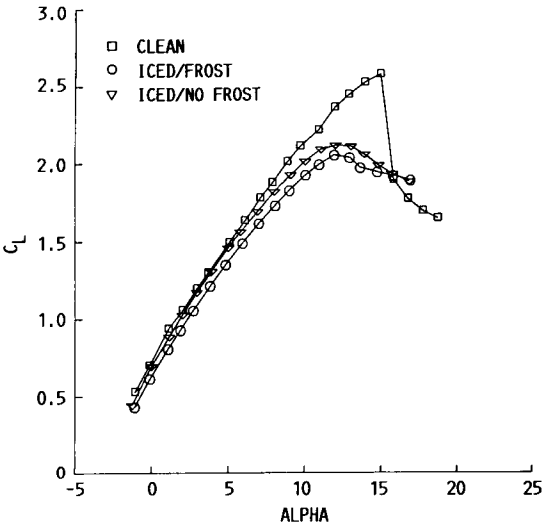

(a) C_L VERSUS AOA.

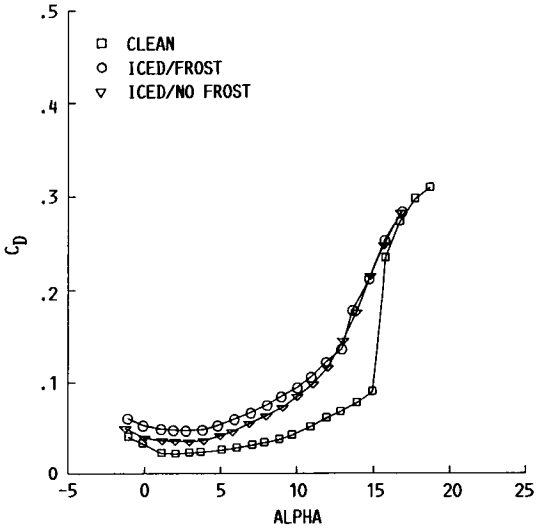

(b) C_D VERSUS AOA.

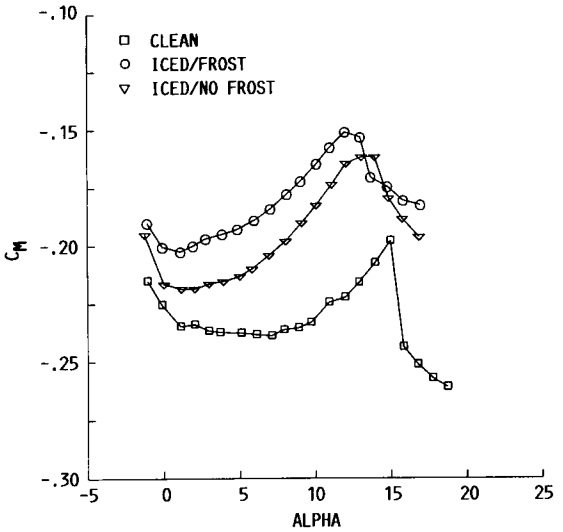

(c) C_M VERSUS AOA.

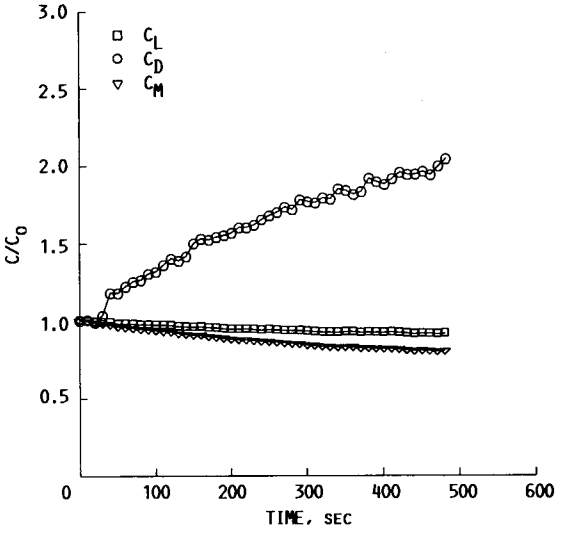

(d) RATIO OF FORCE COEFFICIENTS/FORCE COEFFICIENT OF CLEAN AIRFOIL VERSUS TIME.

FIGURE 16. - ICE SHAPE TRACINGS AND FORCE BALANCE MEASUREMENTS FOR RUN NUMBER 14.

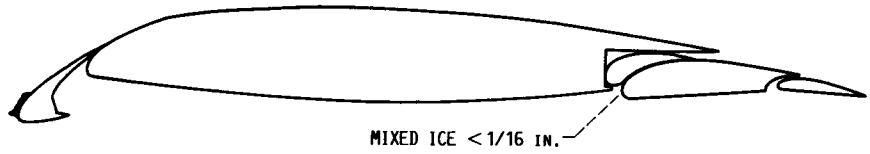

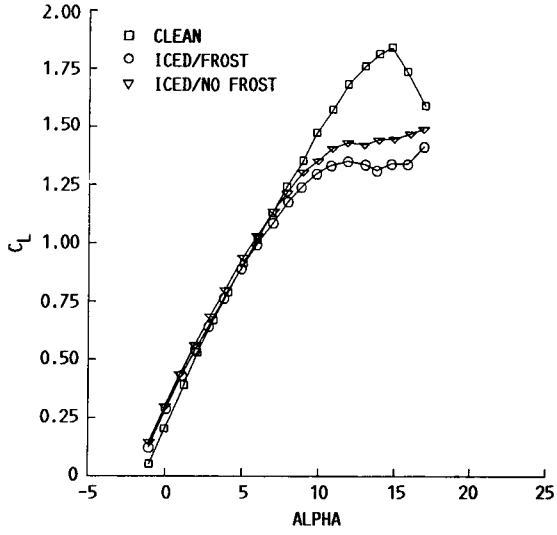

(a) C_L VERSUS AOA.

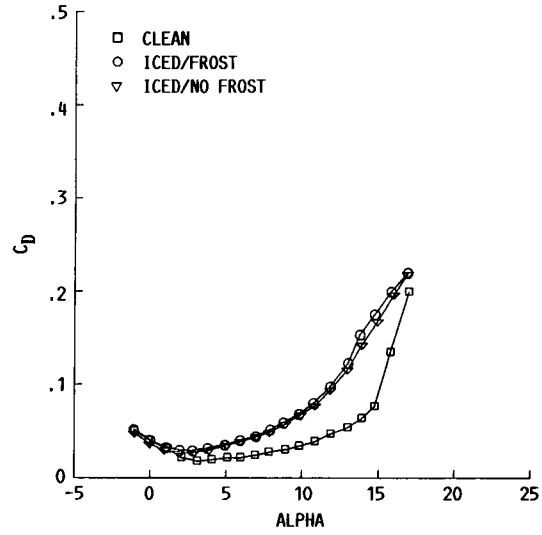

(b) C_D VERSUS AOA.

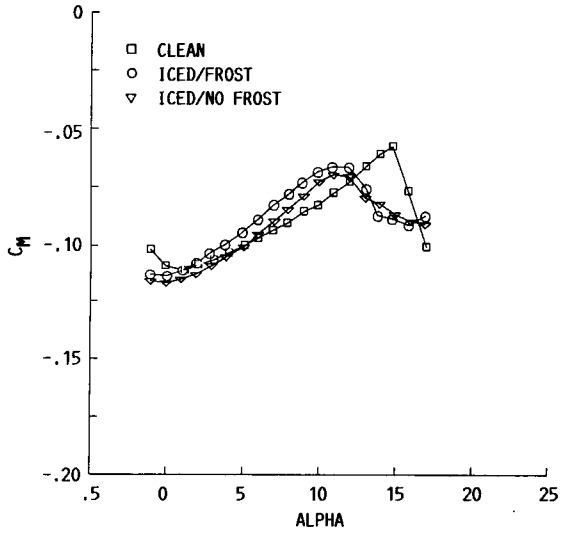

(c) C_M VERSUS AOA.

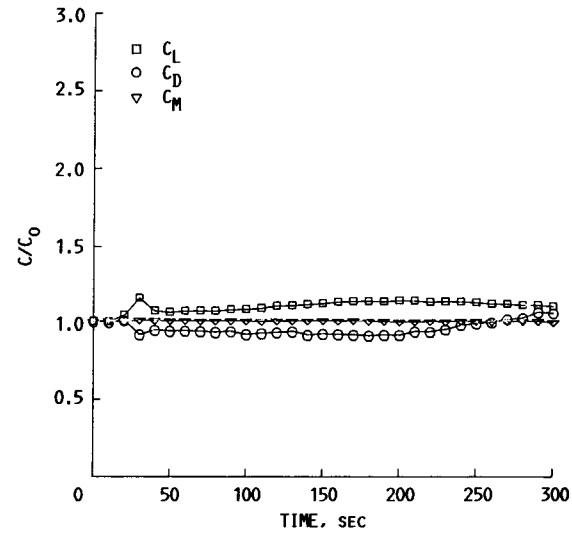

(d) RATIO OF FORCE COEFFICIENTS/FORCE COEFFICIENT OF CLEAN AIRFOIL VERSUS TIME.

FIGURE 17. - ICE SHAPE TRACINGS AND FORCE BALANCE MEASUREMENTS FOR RUN NUMBER 15.

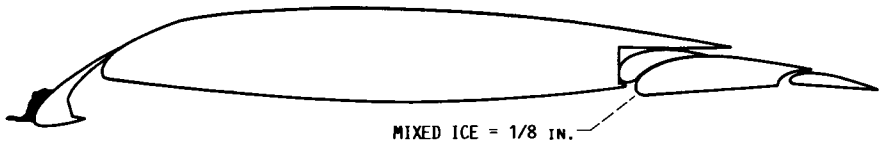

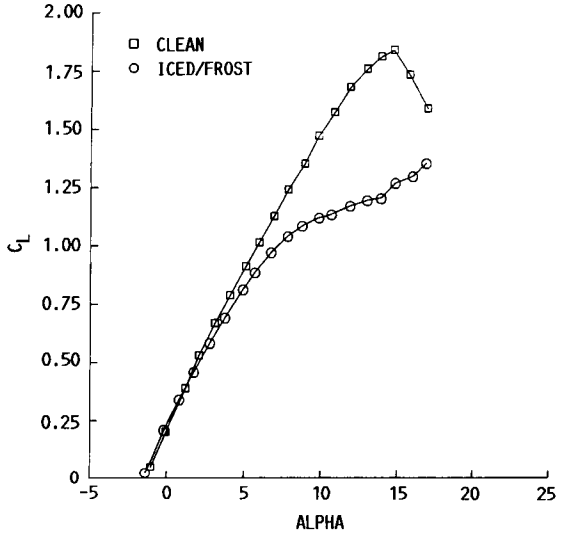

(a) C_L VERSUS AOA.

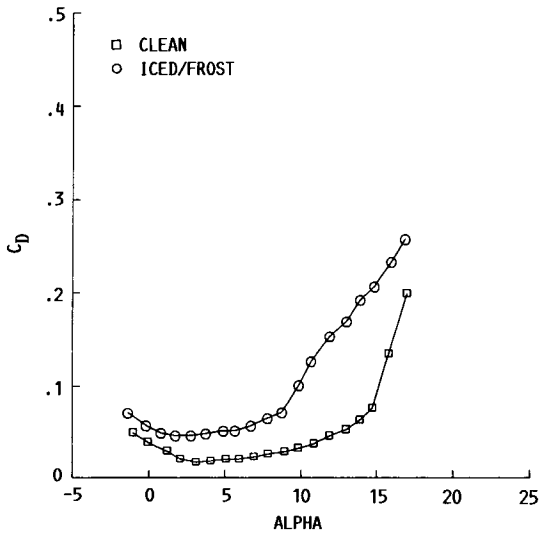

(b) C_D VERSUS AOA.

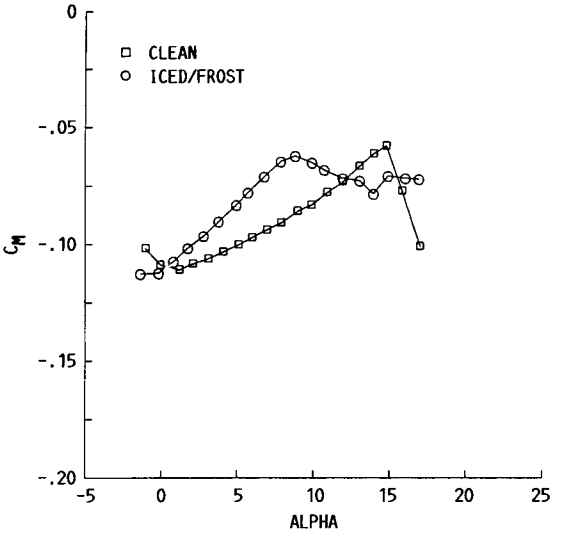

(c) C_M VERSUS AOA.

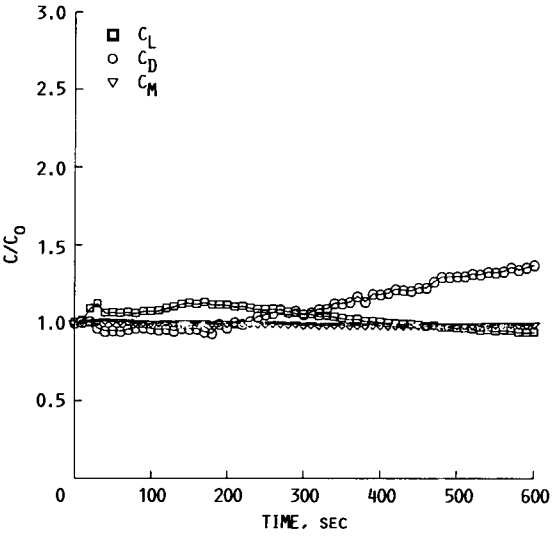

(d) RATIO OF FORCE COEFFICIENTS/FORCE COEFFICIENT OF CLEAN AIRFOIL VERSUS TIME.

FIGURE 18. - ICE SHAPE TRACINGS AND FORCE BALANCE MEASUREMENTS FOR RUN NUMBER 16.

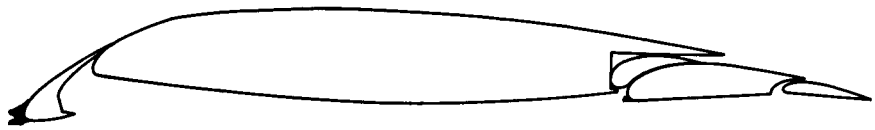

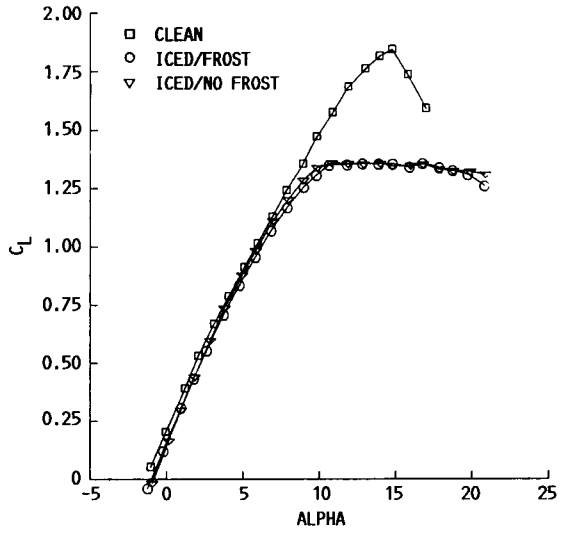

(a) C_L VERSUS AOA.

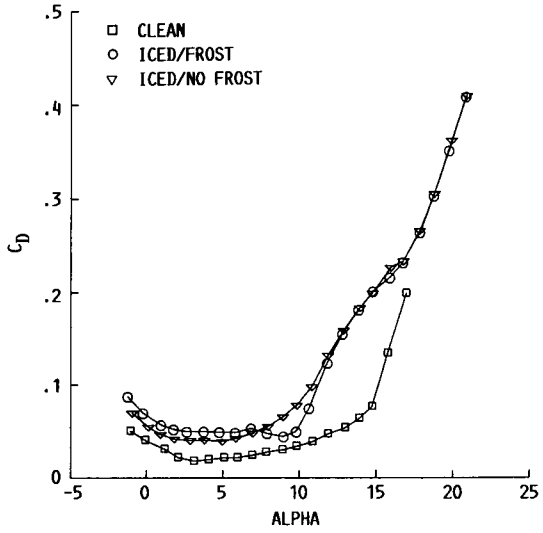

(b) C_D VERSUS AOA.

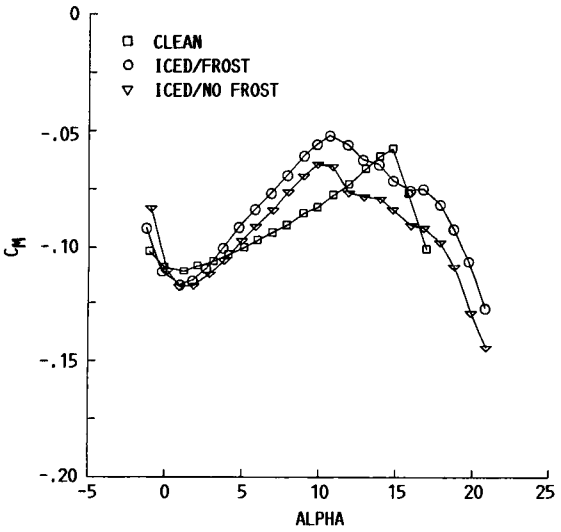

(c) C_M VERSUS AOA.

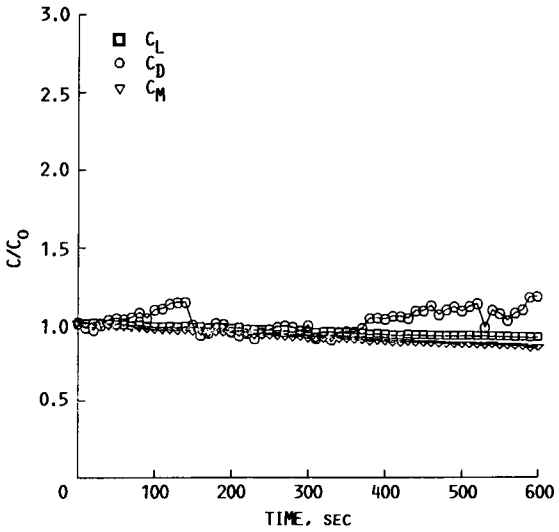

(d) RATIO OF FORCE COEFFICIENTS/FORCE COEFFICIENT OF CLEAN AIRFOIL VERSUS TIME.

FIGURE 19. - ICE SHAPE TRACINGS AND FORCE BALANCE MEASUREMENTS FOR RUN NUMBER 17.

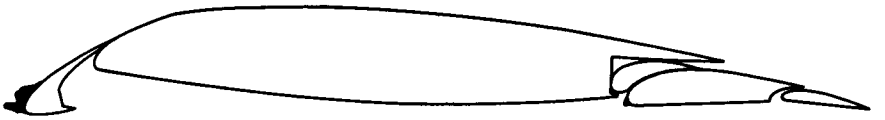

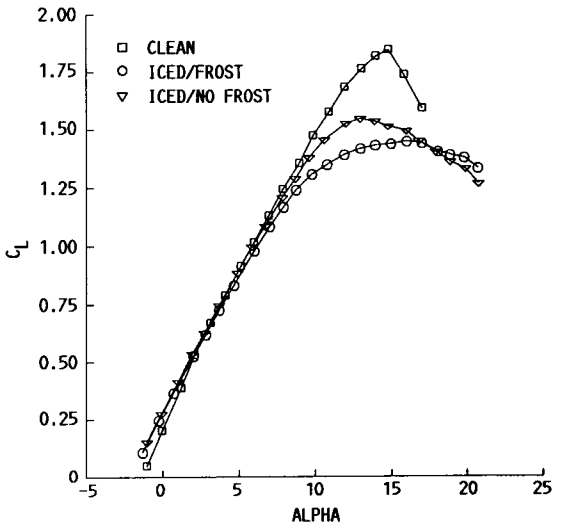

(a) C_L VERSUS AOA.

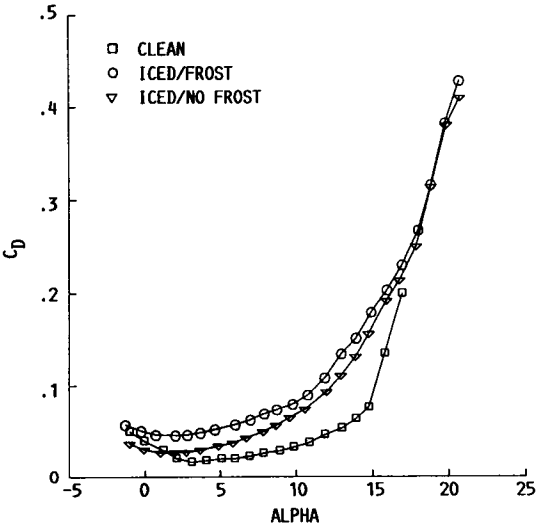

(b) C_D VERSUS AOA.

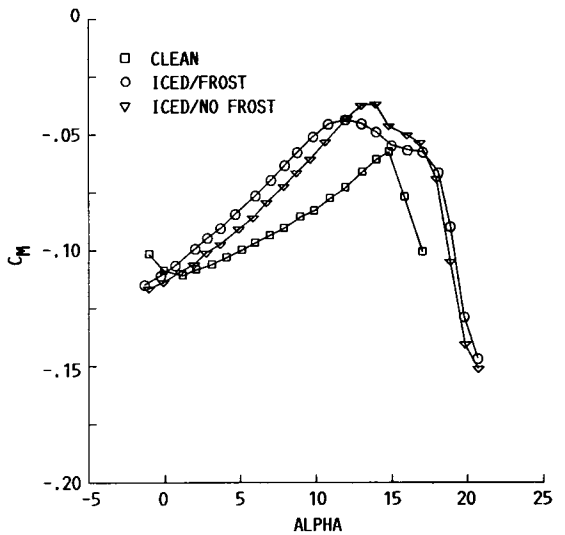

(c) C_M VERSUS AOA.

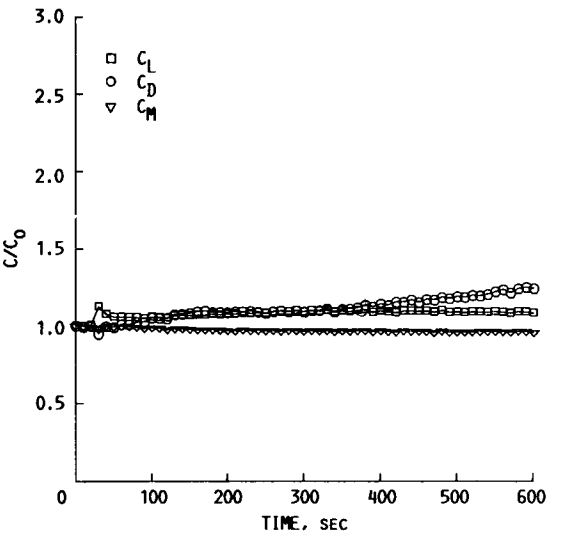

(d) RATIO OF FORCE COEFFICIENTS/FORCE COEFFICIENT OF CLEAN AIRFOIL VERSUS TIME.

FIGURE 20. - ICE SHAPE TRACINGS AND FORCE BALANCE MEASUREMENTS FOR RUN NUMBER 18.

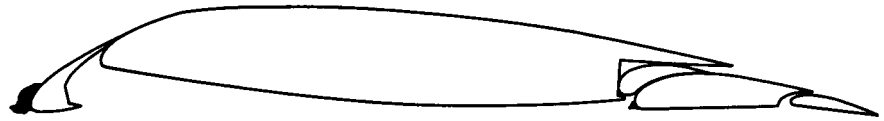

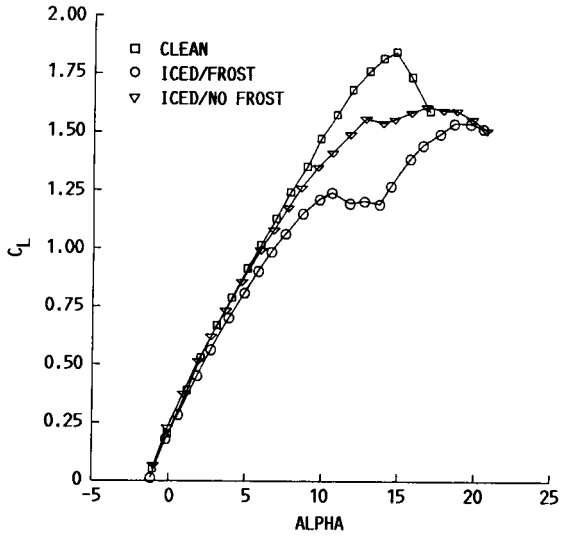

(a) C_L VERSUS AOA.

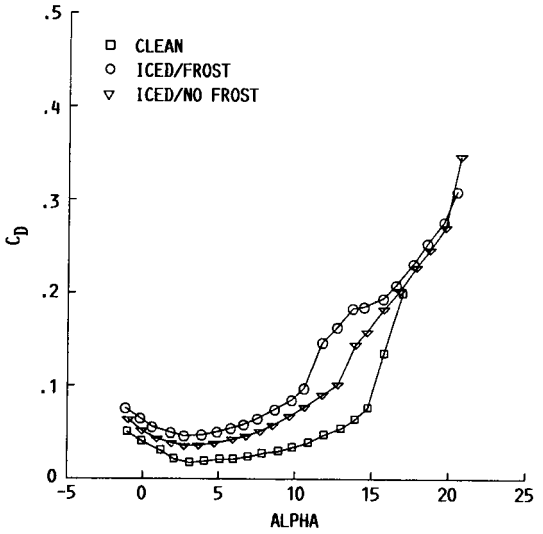

(b) C_D VERSUS AOA.

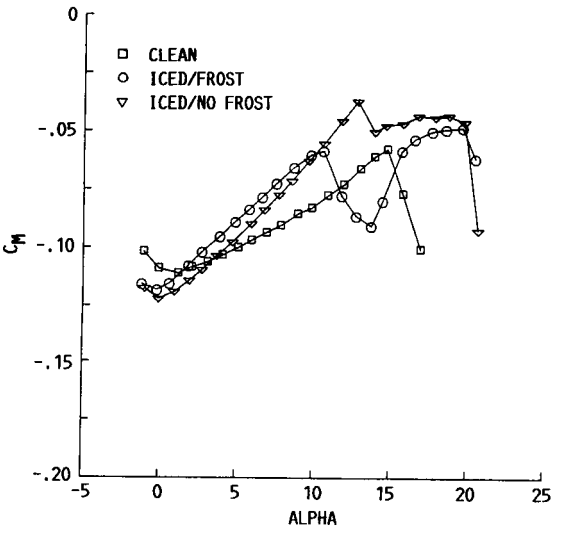

(c) C_M VERSUS AOA.

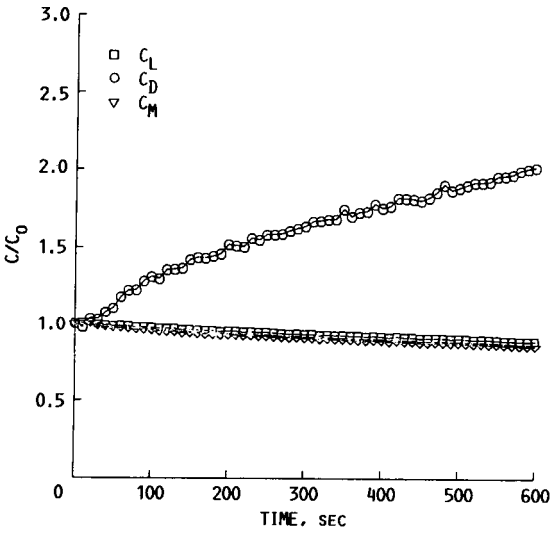

(d) RATIO OF FORCE COEFFICIENTS/FORCE COEFFICIENT OF CLEAN AIRFOIL VERSUS TIME.

FIGURE 21. - ICE SHAPE TRACINGS AND FORCE BALANCE MEASUREMENTS FOR RUN NUMBER 19.

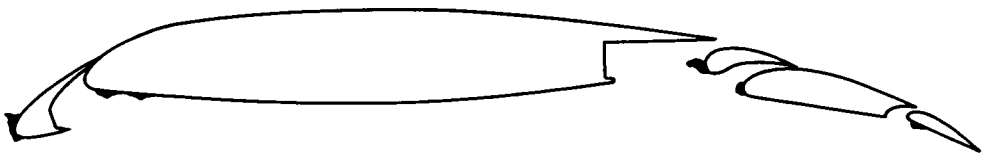

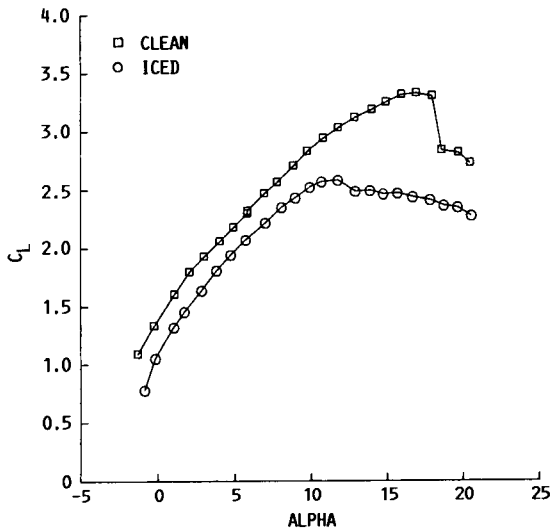

(a) C_L VERSUS AOA.

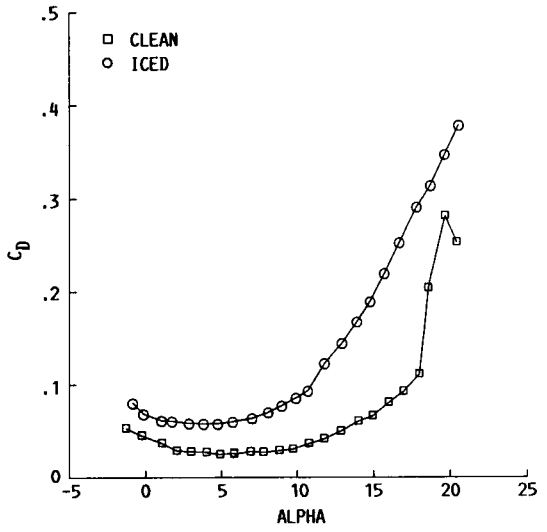

(b) C_D VERSUS AOA.

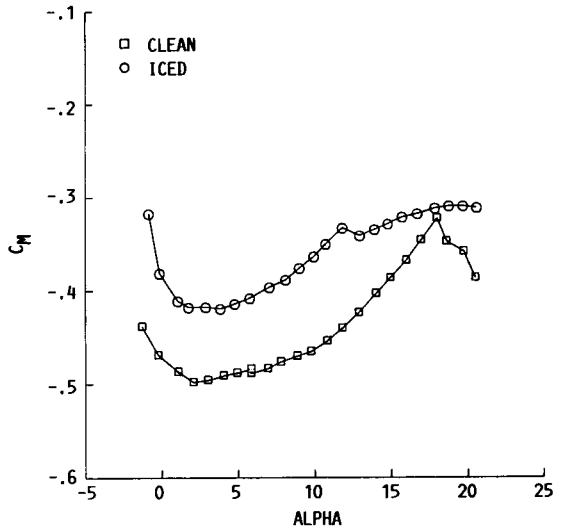

(c) C_M VERSUS AOA.

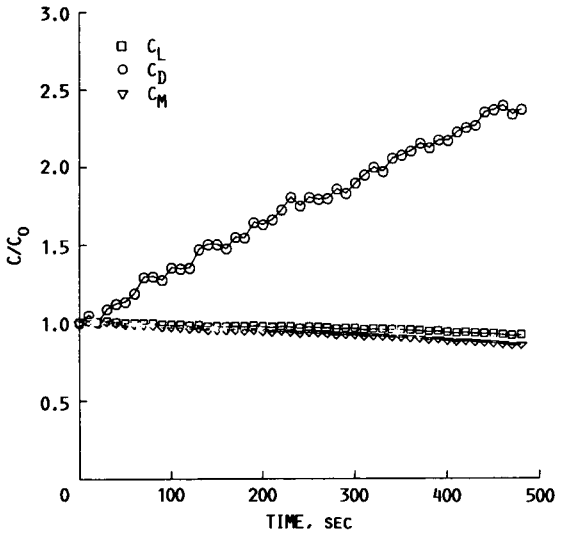

(d) RATIO OF FORCE COEFFICIENTS/FORCE COEFFICIENT OF CLEAN AIRFOIL VERSUS TIME.

FIGURE 22. - ICE SHAPE TRACINGS AND FORCE BALANCE MEASUREMENTS FOR RUN NUMBER 21.

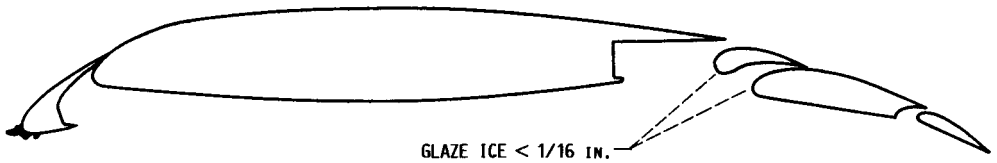

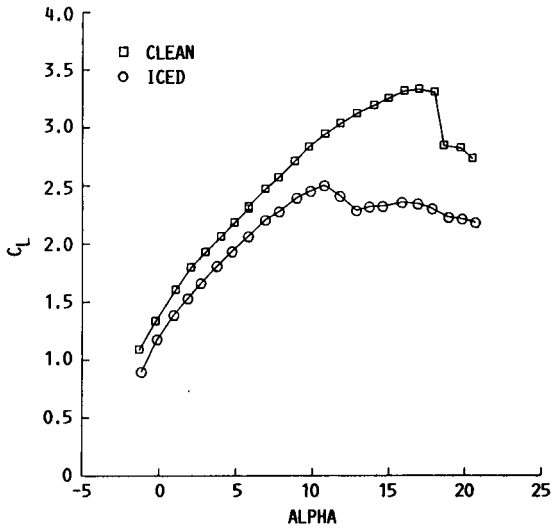

(a) C_L VERSUS AOA.

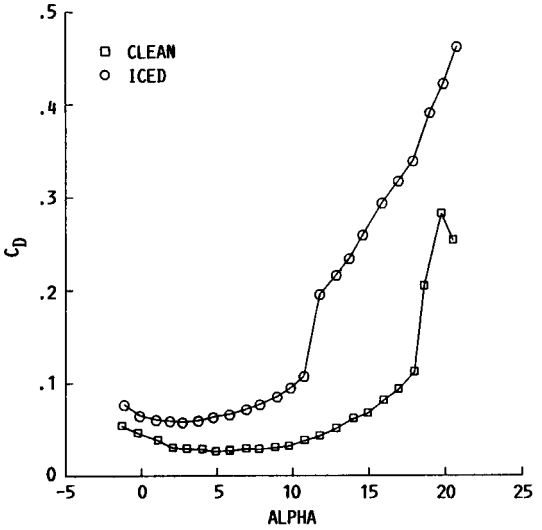

(b) C_D VERSUS AOA.

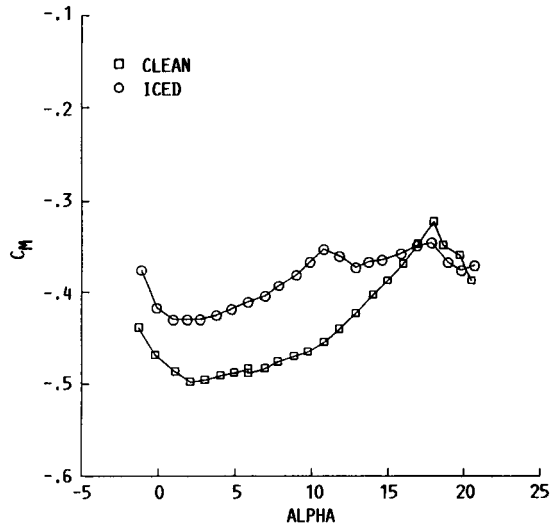

(c) C_M VERSUS AOA.

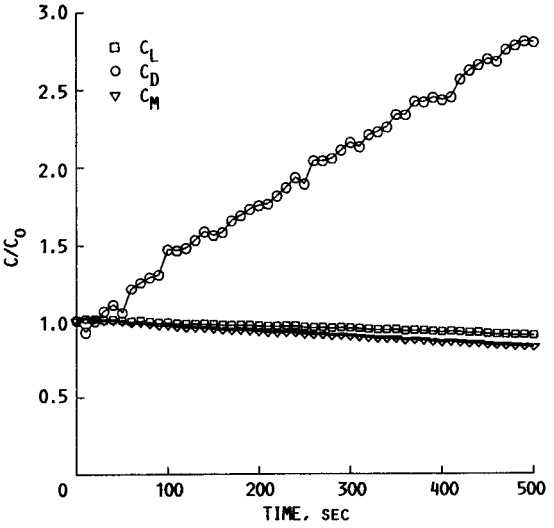

(d) RATIO OF FORCE COEFFICIENT/FORCE COEFFICIENT OF CLEAN AIRFOIL VERSUS TIME.

FIGURE 23. - ICE SHAPE TRACINGS AND FORCE BALANCE MEASUREMENTS FOR RUN NUMBER 22.

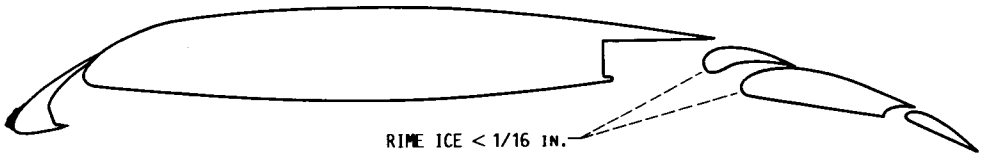

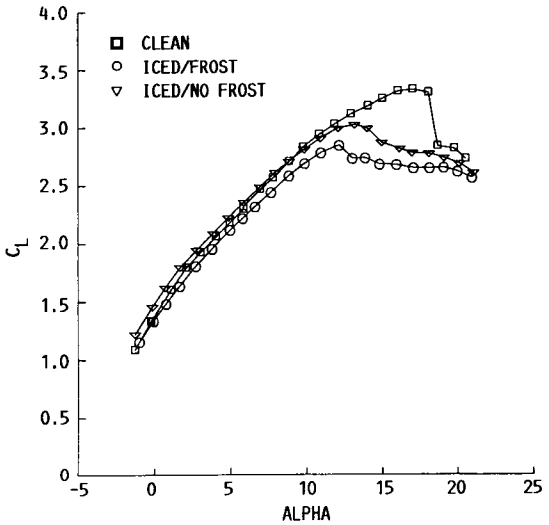

(a) C_L VERSUS AOA.

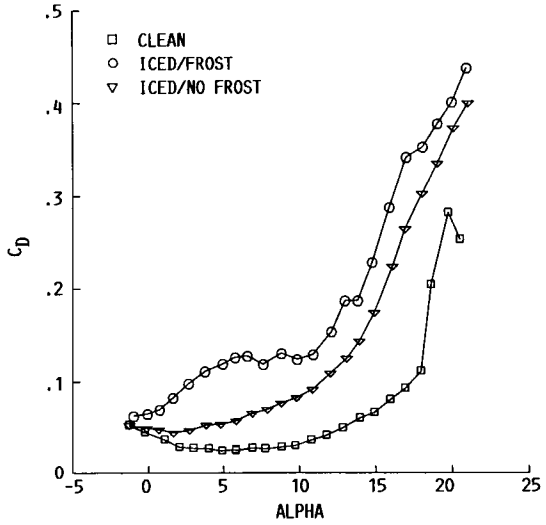

(b) C_D VERSUS AOA.

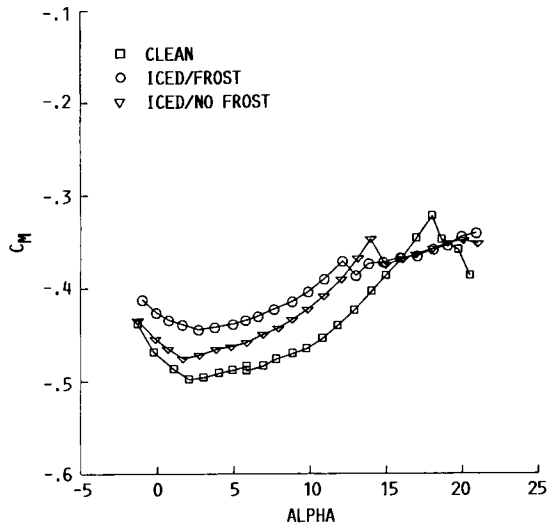

(c) C_M VERSUS AOA.

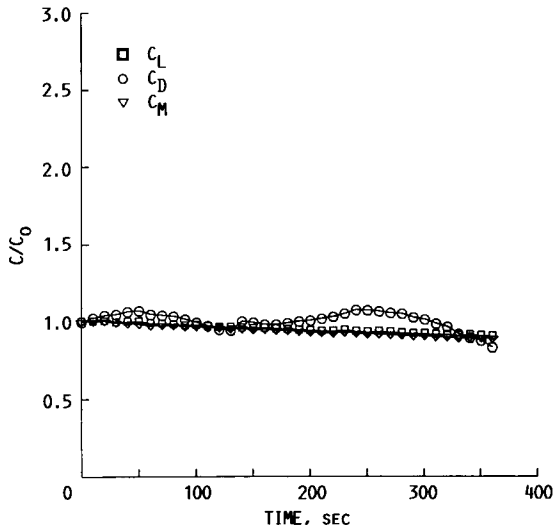

(d) RATIO OF FORCE COEFFICIENTS/FORCE COEFFICIENT OF CLEAN AIRFOIL VERSUS TIME.

FIGURE 24. - ICE SHAPE TRACINGS AND FORCE BALANCE MEASUREMENTS FOR RUN RUNNER 23.

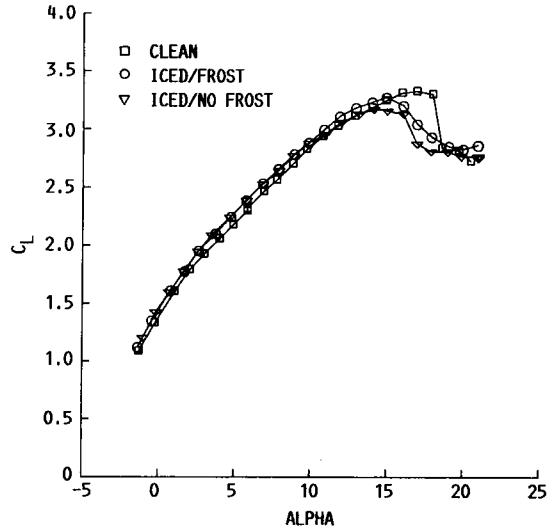

(a) C_L VERSUS AOA.

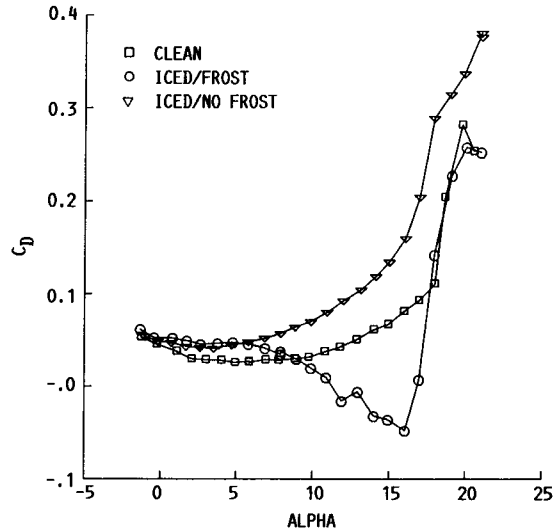

(b) C_D VERSUS AOA.

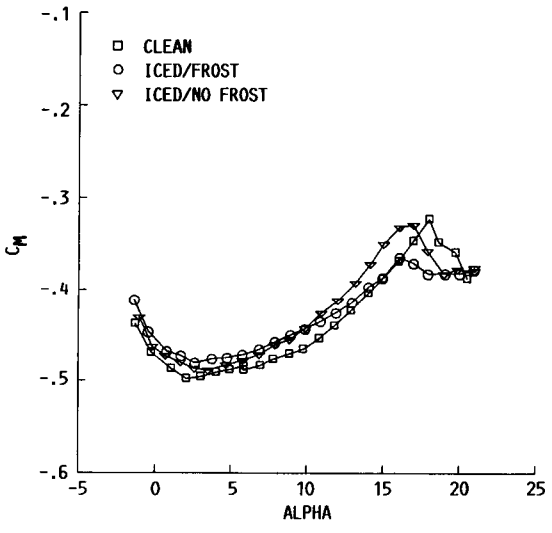

(c) C_M VERSUS AOA.

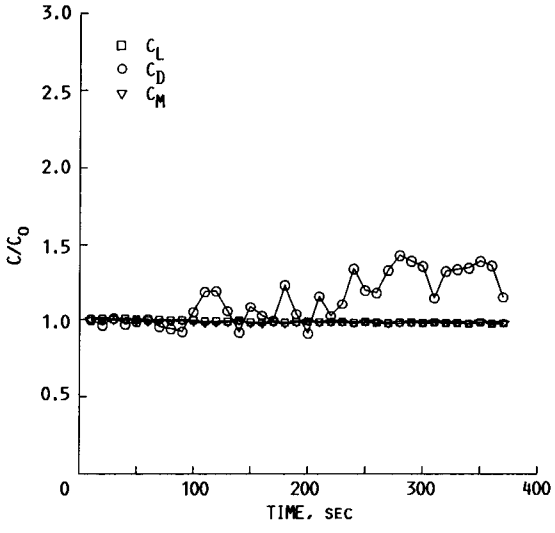

(d) RATIO OF FORCED COEFFICIENTS/FORCE COEFFICIENT OF CLEAN AIRFOIL VERSUS TIME.

FIGURE 25. - ICE SHAPE TRACINGS AND FORCE BALANCE MEASUREMENTS FOR RUN NUMBER 24.

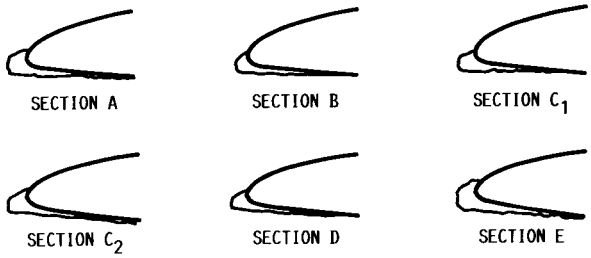

(a) ICE SHAPE TRACINGS FOR SECTION a-e.

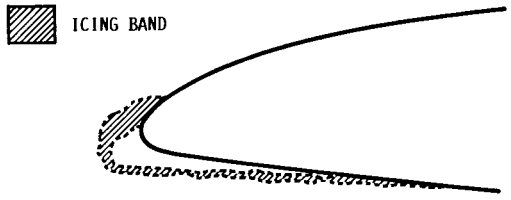

(b) COMPOSITE OF ICE SHAPE TRACINGS SHOWING ICING BAND.

FIGURE 26. - SPANWISE VARIATION IN ICE SHAPES FOR RUN 4b.

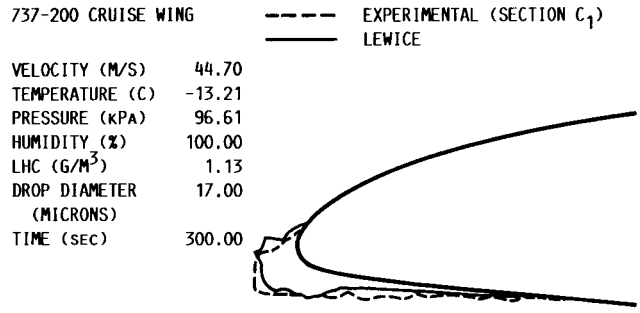

(a) LEWICE COMPARISON WITH SECTION C_1.

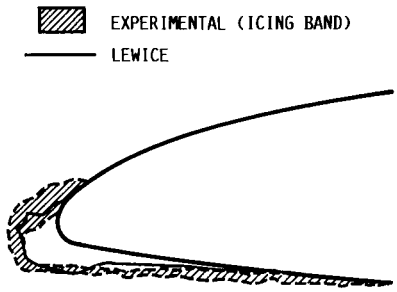

(b) LEWICE COMPARISON WITH ICING BAND.

FIGURE 27. - LEWICE COMPARISON WITH EXPERIMENTAL RESULTS FOR RUN 4b.

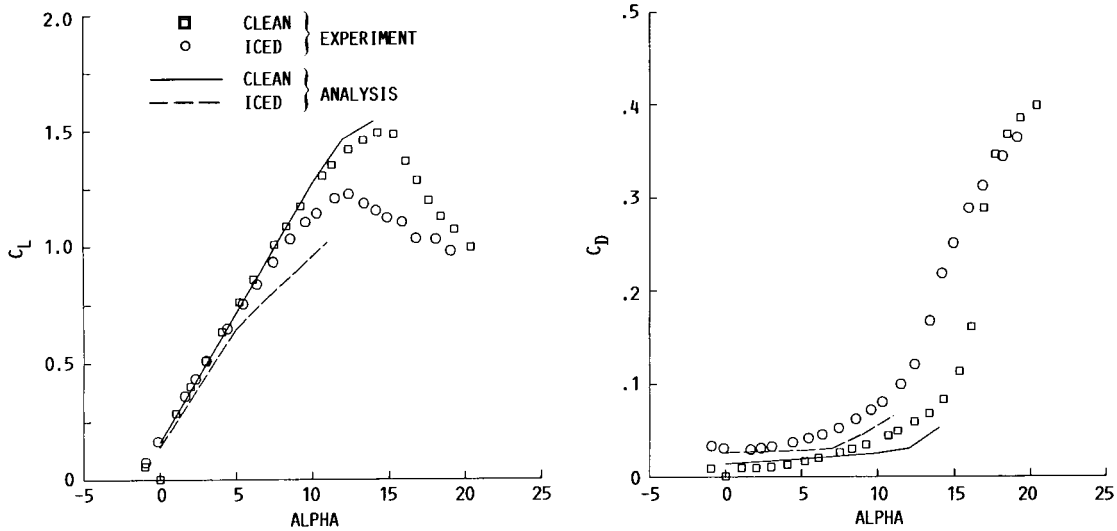

FIGURE 28. - FORCE COEFFICIENT COMPARISONS BETWEEN EXPERIMENTAL RESULTS AND ANALYSIS FOR CRUISE WING CONFIGURATION, CLEAN AND ICED. ICED CONDITION IS RUN 4b.

NASA
National Aeronautics and Space Administration

Report Documentation Page

1. Report No.	2. Government Accession No.	3. Recipient's Catalog No.
NASA TM-101441 AIAA-89-0752		

4. Title and Subtitle

An Experimental Investigation of Multi-Element Airfoil Ice Accretion and Resulting Performance Degradation

5. Report Date

6. Performing Organization Code

7. Author(s)

Mark G. Potapczuk and Brian M. Berkowitz

8. Performing Organization Report No.

E-4546

10. Work Unit No.

505-68-11

9. Performing Organization Name and Address

National Aeronautics and Space Administration
Lewis Research Center
Cleveland, Ohio 44135-3191

11. Contract or Grant No.

13. Type of Report and Period Covered

Technical Memorandum

12. Sponsoring Agency Name and Address

National Aeronautics and Space Administration
Washington, D.C. 20546-0001

14. Sponsoring Agency Code

15. Supplementary Notes

Prepared for the 27th Aerospace Sciences Meeting sponsored by the American Institute of Aeronautics and Astronautics, Reno, Nevada, January 9-12, 1989. Mark G. Potapczuk, NASA Lewis Research Center; Brian M. Berkowitz, Sverdrup Technology, Inc., NASA Lewis Research Center Group, Cleveland, Ohio 44135.

16. Abstract

An investigation of the ice accretion patterns and performance characteristics of a multi-element airfoil was undertaken in the NASA Lewis 6- by 9-Foot Icing Research Tunnel. Several configurations of main airfoil, slat, and flaps were employed to examine the effects of ice accretion and provide further experimental information for code validation purposes. The test matrix consisted of glaze, rime, and mixed icing conditions. Airflow and icing cloud conditions were set to correspond to those typical of the operating environment anticipated for a commercial transport vehicle. Results obtained included ice profile tracings, photographs of the ice accretions, and force balance measurements obtained both during the accretion process and in a post-accretion evaluation over a range of angles of attack. The tracings and photographs indicated significant accretions on the slat leading edge, in gaps between slat or flaps and the main wing, on the flap leading edge surfaces, and on flap lower surfaces. Force measurements indicate the possibility of severe performance degradation, especially near C_{Lmax}, for both light and heavy ice accretions. Frost was also seen on the lower surface of the airfoil. This frost is considered to be a phenomena inherent to the IRT and is not seen in natural icing. The contribution of frost to the force components was evaluated and found to be significant. The cruise wing configuration provided a test case for evaluation of the ice accretion and performance analysis codes presently in use. The LEWICE code was used to evaluate the ice accretion shape developed during one of the rime ice tests. The actual ice shape was then evaluated, using a Navier-Stokes code, for changes in performance characteristics. These predicted results were compared to the measured results and indicate very good agreement.

17. Key Words (Suggested by Author(s))	18. Distribution Statement
Aircraft icing Aerodynamic modeling	Unclassified – Unlimited Subject Category 02

19. Security Classif. (of this report)	20. Security Classif. (of this page)	21. No of pages	22. Price*
Unclassified	Unclassified	40	A03

*For sale by the National Technical Information Service, Springfield, Virginia 22161